SN 2010ay IS A LUMINOUS AND BROAD-LINED TYPE Ic SUPERNOVA WITHIN A LOW-METALLICITY HOST GALAXY

N. E. SANDERS[1], A. M. SODERBERG[1], S. VALENTI[2], R. J. FOLEY[1], R. CHORNOCK[1], L. CHOMIUK[1,3,18], E. BERGER[1], S. SMARTT[2], K. HURLEY[4], S. D. BARTHELMY[5], E. M. LEVESQUE[6], G. NARAYAN[7], M. T. BOTTICELLA[2], M. S. BRIGGS[8], V. CONNAUGHTON[8], Y. TERADA[9], N. GEHRELS[5], S. GOLENETSKII[10], E. MAZETS[10], T. CLINE[5,19], A. VON KIENLIN[11], W. BOYNTON[12], K. C. CHAMBERS[13], T. GRAV[14], J. N. HEASLEY[13], K. W. HODAPP[13], R. JEDICKE[13], N. KAISER[13], R. P. KIRSHNER[1], R.-P. KUDRITZKI[13], G. A. LUPPINO[13], R. H. LUPTON[15], E. A. MAGNIER[13], D. G. MONET[16], J. S. MORGAN[13], P. M. ONAKA[13], P. A. PRICE[15], C. W. STUBBS[7], J. L. TONRY[13], R. J. WAINSCOAT[13], AND M. F. WATERSON[17]

[1] Harvard-Smithsonian Center for Astrophysics, 60 Garden Street, Cambridge, MA 02138, USA; nsanders@cfa.harvard.edu
[2] Astrophysics Research Centre, School of Maths and Physics, Queen's University, Belfast BT7 1NN, UK
[3] National Radio Astronomy Observatory, Socorro, NM 87801, USA
[4] Space Sciences Laboratory, University of California Berkeley, 7 Gauss Way, Berkeley, CA 94720, USA
[5] NASA Goddard Space Flight Center, Code 661, Greenbelt, MD 20771, USA
[6] CASA, Department of Astrophysical and Planetary Sciences, University of Colorado, 389-UCB, Boulder, CO 80309, USA
[7] Department of Physics, Harvard University, Cambridge, MA 02138, USA
[8] CSPAR, University of Alabama in Huntsville, Huntsville, AL, USA
[9] Department of Physics, Saitama University, Shimo-Okubo, Sakura-ku, Saitama-shi, Saitama 338-8570, Japan
[10] Ioffe Physico-Technical Institute, Laboratory for Experimental Astrophysics, 26 Polytekhnicheskaya, St. Petersburg 194021, Russia
[11] Max-Planck Institut für extraterrestrische Physik, D-85748 Garching, Germany
[12] Lunar and Planetary Laboratory, University of Arizona, Tucson, AZ 85721, USA
[13] Institute for Astronomy, University of Hawaii at Manoa, Honolulu, HI 96822, USA
[14] Planetary Science Institute, 1700 East Fort Lowell, Suite 106, Tucson, AZ 85919, USA
[15] Department of Astrophysical Sciences, Princeton University, Princeton, NJ 08544, USA
[16] US Naval Observatory, Flagstaff Station, Flagstaff, AZ 86001, USA
[17] International Center for Radio Astronomy Research, The University of Western Australia, Crawley, Perth, Australia

ABSTRACT

We report on our serendipitous pre-discovery detection and follow-up observations of the broad-lined Type Ic supernova (SN Ic) 2010ay at $z = 0.067$ imaged by the Pan-STARRS1 3π survey just ∼4 days after explosion. The supernova (SN) had a peak luminosity, $M_R \approx -20.2$ mag, significantly more luminous than known GRB–SNe and one of the most luminous SNe Ib/c ever discovered. The absorption velocity of SN 2010ay is $v_{\rm Si} \approx 19 \times 10^3$ km s^{-1} at ∼40 days after explosion, 2–5 times higher than other broad-lined SNe and similar to the GRB–SN 2010bh at comparable epochs. Moreover, the velocity declines ∼2 times slower than other SNe Ic-BL and GRB–SNe. Assuming that the optical emission is powered by radioactive decay, the peak magnitude implies the synthesis of an unusually large mass of ^{56}Ni, $M_{\rm Ni} = 0.9\,M_\odot$. Applying scaling relations to the light curve, we estimate a total ejecta mass, $M_{\rm ej} \approx 4.7\,M_\odot$, and total kinetic energy, $E_K \approx 11 \times 10^{51}$ erg. The ratio of $M_{\rm Ni}$ to $M_{\rm ej}$ is ∼2 times as large for SN 2010ay as typical GRB–SNe and may suggest an additional energy reservoir. The metallicity $(\log({\rm O/H})_{\rm PP04} + 12 = 8.19)$ of the explosion site within the host galaxy places SN 2010ay in the low-metallicity regime populated by GRB–SNe, and ∼0.5(0.2) dex lower than that typically measured for the host environments of normal (broad-lined) SNe Ic. We constrain any gamma-ray emission with $E_\gamma \lesssim 6 \times 10^{48}$ erg (25–150 keV), and our deep radio follow-up observations with the Expanded Very Large Array rule out relativistic ejecta with energy $E \gtrsim 10^{48}$ erg. We therefore rule out the association of a relativistic outflow like those that accompanied SN 1998bw and traditional long-duration gamma-ray bursts (GRBs), but we place less-stringent constraints on a weak afterglow like that seen from XRF 060218. If this SN did not harbor a GRB, these observations challenge the importance of progenitor metallicity for the production of relativistic ejecta and suggest that other parameters also play a key role.

Key words: gamma-ray burst: general – supernovae: general – supernovae: individual (2010ay)

Online-only material: color figures

1. INTRODUCTION

Recent observations have shown that long-duration gamma-ray bursts (GRBs) are accompanied by Type Ic supernovae (SNe Ic) with broad absorption features (hereafter "broad-lined," BL) indicative of high photospheric expansion velocities (see Woosley & Bloom 2006, for a review). This GRB–SN connection is popularly explained by the favored "collapsar model" (MacFadyen et al. 2001) in which the gravitational collapse of a massive ($M \gtrsim 20\,M_\odot$) progenitor star gives birth to a central engine—a rapidly rotating and accreting compact object—that powers a relativistic outflow. At the same time, not all SNe Ic-BL show evidence for a central engine. Radio observations constrain the fraction of SNe Ic-BL harboring relativistic outflows to be less than a third (Soderberg et al. 2006a, 2010).

---

[18] L.C. is a Jansky Fellow of the National Radio Astronomy Observatory.
[19] Emeritus

The physical parameter(s) that distinguishes the progenitors of GRB-associated SNe from other SNe Ic-BL remains debated, while theoretical considerations indicate that progenitor metallicity may play a key role (Woosley & Heger 2006). In the collapsar scenario, massive progenitor stars with metallicity above a threshold $Z \gtrsim 0.3\,Z_\odot$ lose angular momentum to metal-line-driven winds, preventing the formation of a rapidly rotating compact remnant and, in turn, a relativistic outflow. At the same time, the hydrogen-free spectra of SNe Ic-BL indicate that their stellar envelopes have been stripped prior to explosion, requiring higher metallicities (e.g., $Z \approx Z_\odot$) if due to radiation-driven winds (Woosley et al. 1995). Alternatively, short-period (∼0.1 days) binary interaction may be invoked to spin up stars via tidal forces, as well as cause mass loss via Roche lobe overflow (Podsiadlowski et al. 2004; Fryer & Heger 2005). However, even in the binary scenario, GRB formation is predicted to occur at higher rates in lower metallicity environments, where the radius and mass-loss rates of stars should be smaller (Izzard et al. 2004).

Observationally, *most* GRB–SNe are discovered within dwarf star-forming galaxies (Fruchter et al. 2006) characterized by sub-solar metallicities, $Z \lesssim 0.5\,Z_\odot$ (Levesque et al. 2010a). This has been interpreted as observational support for the metallicity-dependent collapsar model (Stanek et al. 2006). Meanwhile, it was noted early on that SNe Ic-BL without associated GRBs have been found in more enriched environments (e.g., Modjaz et al. 2008; Prieto et al. 2008), motivating the suggestion of an observationally determined cutoff metallicity above which GRB–SNe do not form (Kocevski et al. 2009). This metallicity difference may be partly attributable to the different survey strategies: SNe have been primarily discovered by galaxy-targeted surveys biased toward more luminous (and therefore higher metallicity) environments, while GRB host galaxies are found in an untargeted manner through their gamma-ray emission (Stanek et al. 2006).

Against this backdrop of progress, recent observations have begun to call into question some aspects of this scenario. First, there are two reported long-duration GRBs in solar or super-solar metallicity environments (GRB 020819, Levesque et al. 2010c; GRB 051022, Graham et al. 2009). Similarly, the luminous radio emission seen from SN Ic-BL 2009bb pointed unequivocally to the production of copious relativistic ejecta resembling a GRB afterglow (Soderberg et al. 2010), while the explosion environment was characterized by a super-solar metallicity, $Z \sim 1$–$2\,Z_\odot$ (Levesque et al. 2010b). Together with the growing lack of evidence for massive progenitor stars for SNe Ic in pre-explosion *Hubble Space Telescope* images (Smartt 2009), a lower mass ($M \sim 10$–$20\,M_\odot$) binary progenitor system model (with a gentler metallicity dependence) is gaining increasing popularity (Yoon et al. 2010). Multi-wavelength studies of SNe Ic-BL in metal-poor environments may shed further light on the role of metallicity in the nature of the progenitor and the explosion properties, including the production of relativistic ejecta.

Fortunately, with the recent advent of wide-field optical transient surveys (e.g., Catalina Real-time Transient Survey (CRTS), Drake et al. 2009; Panchromatic Survey Telescope and Rapid Response System (Pan-STARRS1, abbreviated PS1), Kaiser et al. 2002; Palomar Transient Factory, Law et al. 2009) SNe Ic-BL are now being discovered in metal-poor environments, $Z \sim 0.5\,Z_\odot$, thanks to an unbiased search technique (see, e.g., Stanek et al. 2006; Modjaz et al. 2008, 2011; Young et al. 2008; Arcavi et al. 2010; Leloudas et al. 2011; Kelly

Table 1
SN 2010ay Host Galaxy SDSS J123527.19+270402.7

Parameter	Value
R.A.	$12^h35^m27^s.19$ (J2000)
Decl.	$+27°04'02''.7$ (J2000)
Redshift (z)	0.0671
Petrosian radius	$1''.355$
Photometry[a]	
u'	19.56 ± 0.03 mag
g'	19.02 ± 0.01 mag
r'	19.02 ± 0.01 mag
i'	18.69 ± 0.01 mag
z'	18.87 ± 0.04 mag
U	19.50 ± 0.06 mag
B	19.02 ± 0.05 mag
V	19.13 ± 0.05 mag
R	18.94 ± 0.05 mag
I	18.90 ± 0.06 mag
Extinction	
$E(B-V)_{\mathrm{MW}}$[b]	0.017 mag
$E(B-V)_{\mathrm{host}}$[c]	0.2 mag

Notes. SDSS host galaxy properties and *ugriz* photometry.
[a] Model magnitudes from SDSS DR8 (Aihara et al. 2011). Host galaxy photometry has not been corrected for extinction. *UBVRI* photometry has been converted from the SDSS *ugriz* measurements using the transformation of Blanton & Roweis (2007).
[b] The Milky Way extinction as determined by Schlegel et al. (1998), assuming $R_V = 3.1$.
[c] The host galaxy extinction determined from the SDSS spectrum centered on the galaxy nucleus, via the Balmer decrement as described in Section 2.3.1.

& Kirshner 2011; Sanders et al. 2012; Stoll et al. 2012). In this paper, we present pre-discovery Pan-STARRS1 imaging and multi-wavelength follow-up observations for the broad-lined Type Ic SN 2010ay discovered by CRTS (Drake et al. 2010). In Section 2, we report our optical (Pan-STARRS1, Gemini, and William Herschel Telescope (WHT)) and radio (Expanded Very Large Array (EVLA)) observations. In Section 3, we model the optical light curve and analyze the spectra to derive the explosion properties of SN 2010ay. In Section 4, we use our observations of SN 2010ay with the EVLA to place strict limits on the presence of relativistic outflow. In Section 5, we draw from gamma-ray satellite coverage to rule out a *detected* GRB in association with SN 2010ay. In Section 6, we derive the explosion site metallicity and find it to be significantly sub-solar and typical of most GRB–SN host environments. In Section 7, we discuss the implications of these findings in the context of the explosion and progenitor properties and conclude in Section 8.

2. OBSERVATIONS

2.1. Discovery by CRTS

SN 2010ay was discovered by the CRTS (Drake et al. 2009) on 2010 March 17.38 UT (Drake et al. 2010) and designated CSS100317:123527+270403, with an unfiltered magnitude of $m \approx 17.5$ mag and located $\lesssim 1''$ of the center of a compact galaxy, SDSS J123527.19+270402.7, at $z = 0.067$ (Table 1). We adopt a distance $D_L = 297.9$ Mpc to the host galaxy[20]

---

[20] We assume $H_0 = 71$ km s^{-1} Mpc^{-1}, $\Omega_\Lambda = 0.73$, and $\Omega_M = 0.27$.
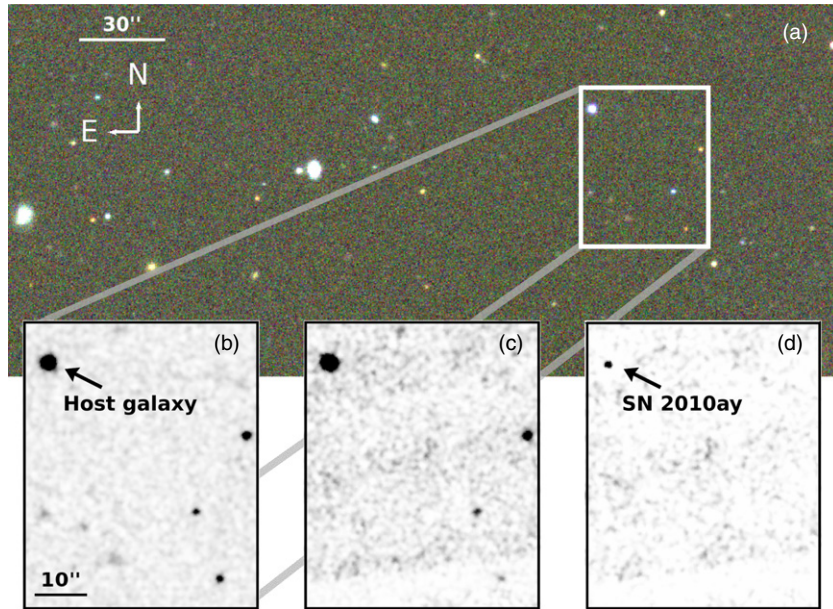
Figure 1. Images illustrating the Pan-STARRS1 pre-discovery detection of SN 2010ay and the surrounding field. (a) Pre-explosion gri-composite image from the SDSS DR7 (Abazajian et al. 2009), observed 2004 December 21, (b) SDSS i-band image geometrically registered to the PS1 image frames and zoomed in to the host galaxy of SN 2010ay, (c) i_{P1}-band image from the 3π survey of PS1, observed 2010 February 25, (d) the difference of the SDSS i' and PS1 i_{P1} images. The transient emission can be seen in the NE corner of the last panel. Nearby stars are included in the zoomed-in frames to illustrate the efficiency of subtraction.
(A color version of this figure is available in the online journal.)

and note that the Galactic extinction toward this galaxy is $E(B - V) = 0.017$ (Schlegel et al. 1998). Pre-discovery unfiltered images from CRTS revealed an earlier detection of the SN on Mar 5.45 UT at $m \approx 18.2$ mag and a non-detection from February 17.45 UT at $m \gtrsim 18.3$ mag (Drake et al. 2010).

A spectrum obtained on March 22 UT revealed the SN to be of Type Ic with broad features, similar to the GRB-associated SN 1998bw spectrum obtained near maximum light (Filippenko et al. 2010). This classification was confirmed by Prieto (2010), who additionally reported photometry for the SN (see Table 2). After numerically subtracting the host galaxy emission, they estimate an unusually luminous absolute magnitude of $V \approx -19.4$ mag.

2.2. Pre-discovery Detection with Pan-STARRS1 3π

The field of SN 2010ay was serendipitously observed with the PS1 3π survey in the weeks preceding its discovery. Pan-STARRS1 is a wide-field imaging system at Haleakala, Hawaii, dedicated to survey observations (Kaiser et al. 2002). The PS1 optical design (Hodapp et al. 2004) uses a 1.8 m diameter $f/4.4$ primary mirror and a 0.9 m secondary. The telescope illuminates a diameter of $3°\!.3$. The Pan-STARRS1 imager (Tonry & Onaka 2009) comprises a total of 60 4800×4800 pixel detectors, with 10 μm pixels that subtend 0.258 arcsec. The PS1 observations are obtained through a set of five broadband filters designated as g_{P1}, r_{P1}, i_{P1}, z_{P1}, and y_{P1}. These filters are similar to those used in previous surveys, such as Sloan Digital Sky Survey (SDSS; Fukugita et al. 1996). However, the g_{P1} filter extends 20 nm redward of g', the z_{P1} filter is cutoff at 930 nm, and SDSS has no corresponding y_{P1} filter (Stubbs et al. 2010).

The field of SN 2010ay was observed on 2010 February 21 (r_{P1} band) and February 25 (i_{P1} band; Figure 1). On each night, four exposures were collected following the strategy of the PS1-3π survey (K. C. Chambers et al. 2012, in preparation). Following the CRTS discovery and announcement of SN 2010ay, we geometrically registered SDSS pre-explosion images to the PS1

Table 2
SN 2010ay Light-curve Photometry

UT Date	MJD	t_{peak}[a]	Filter	m[b]	M_R[c]	Source
733820.4	55244.4	−29	⋯	<18.3	<−19.2 ± 0.2	d
733824.6	55248.6	−25	r_{P1}	<22.0 ± 0.1	<−16.0 ± 0.1	e
733828.2	55252.2	−21	i_{P1}	21.1 ± 0.3	−16.8 ± 0.3	e
733836.4	55260.4	−13	⋯	18.2	−19.3 ± 0.2	d
733848.4	55272.4	−1	⋯	17.5	−20.4 ± 0.2	d
733853.2	55277.2	4	B	18.39 ± 0.05	⋯	f
733853.2	55277.2	4	V	17.61 ± 0.05	⋯	f
733853.2	55277.2	4	R	17.44 ± 0.05	−20.22 ± 0.07	f
733863.0	55287.0	14	R	18.2 ± 0.2	−19.2 ± 0.2	g
733873.0	55297.0	24	g	18.9 ± 0.1	⋯	h
733873.0	55297.0	24	r	18.3 ± 0.1	−19.0 ± 0.1	h
733873.0	55297.0	24	i	18.0 ± 0.1	⋯	h
734221.0	55645.0	372	i_{P1}	<22.2 ± 0.2	<−16.22 ± 0.10	e
734225.0	55649.0	376	r_{P1}	<21.9 ± 0.1	<−15.7 ± 0.1	e

Notes.
[a] Time since peak in days, relative to the fitted value: 2010 March 18.5 ± 0.2.
[b] The measured apparent magnitude of the source, in the filter noted and without extinction correction. For the Pan-STARRS1 photometry, a template image was subtracted; for the other points, the host galaxy flux has not been subtracted.
[c] The absolute R magnitude of the SN. Filter conversion, host flux subtraction, and extinction correction have been performed as described in Section 3.1.
[d] Drake et al. (2010), unfiltered (synthetic V band).
[e] Photometry from the Pan-STARRS1 3π survey.
[f] Prieto (2010).
[g] Synthetic photometry obtained from our WHT spectrum as described in Section 2.3.
[h] Photometry from our Gemini/GMOS observations described in Section 2.2.

images and performed digital image subtraction using the *ISIS* package (Alard 2000). Photometric calibration was performed using many field stars in the SDSS catalog with magnitudes $r \approx 13$–19 mag. No residual flux was found in the difference r_{P1}-band image from 2010 February 21 with an upper limit of
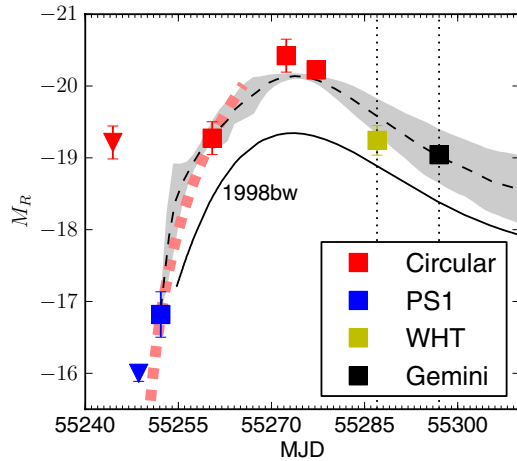
Figure 2. Optical R-band light curve of SN 2010ay, as compiled in Table 2 from CBET 2224 (red squares), the PS1 3π survey (blue), our Gemini images (black), and synthetic photometry (Section 2.3) based on our WHT spectrum (gold). Triangles denote upper limits. The thick dashed line represents the luminosity of an expanding fireball fit to our early-time photometry (Section 3.1). The thin dashed line is the SN Ib/c light-curve template of Drout et al. (2011), and the gray field represents the standard deviation among its constituent photometry. The template is stretched by $(1 + z) = 1.067$ with the best-fit parameters t_{Rpeak} = March 18 $\pm$ 2 (MJD 55273 $\pm$ 2) and $M_{\mathrm{Rpeak}} = -20.2 \pm 0.2$ mag. The solid line is the light curve of the GRB–SN 1998bw (Galama et al. 1998), redshifted to match SN 2010ay. The vertical dotted lines mark the epochs of our Gemini and WHT spectroscopy.

(A color version of this figure is available in the online journal.)

$r > 22.0$ mag. However, we detect residual flux at the position of SN 2010ay in the i_{P1}-band residual image from 2010 February 25 with a magnitude of $i' = 21.1 \pm 0.3$ mag.

The field was again observed in the i_{P1} band on 2011 March 25 and the r_{P1} band on 2011 March 29, but no residual flux was detected in the subtractions at the SN position to limits of $i' \gtrsim 22.2$ and $r' \gtrsim 21.9$.

In Table 2 and Figure 2, we compile photometry from the PS1 detections, our optical observations, and the circulars to construct a light curve for SN 2010ay.

2.3. Optical Observations

We obtained an optical spectrum ($\sim$3000–11000 Å) of SN 2010ay on April 1 UT, from the ISIS blue arm instrument of the 4.2 m WHT at the Roque de Los Muchachos Observatory. The spectrum was taken at the parallactic angle, and the exposure time was 1800 s. We obtained a second 1800 s optical spectrum ($\sim$3600–9600 Å) using the Gemini Multi-Object Spectrograph (GMOS) on the 8.1 m Gemini North telescope on 2010 April 11.4 UT. We employed standard two-dimensional long-slit image reduction and spectral extraction routines in IRAF.[21] We do not apply a correction for atmospheric differential refraction, because the displacement should be $\lesssim 0\rlap{.}{''}5$ at the airmass of the observations, ≈ 1.0.

In both our Gemini and WHT spectra, broad absorption features associated with the SN are clearly detected in addition to narrow emission lines typical of star-forming galaxies. We distinguish the host galaxy emission from the continuum dominated by the highly broadened SN emission by subtracting a high-order spline fit to the continuum. Both SN and host

Table 3
Emission-line Fluxes Measured for the Host Galaxy of SN 2010ay

Emission Line	Flux (10^{-16} erg s^{-1} cm^{-2})
[O II] $\lambda\lambda$3726, 3729	52 $\pm$ 1
Hδ	4.5 $\pm$ 0.2
Hγ	9.9 $\pm$ 0.1
[O III] λ4363	0.7 $\pm$ 0.1
Hβ	24.5 $\pm$ 0.1
[O III] λ4959	30.4 $\pm$ 0.1
[O III] λ5007	90.1 $\pm$ 0.2
[N II] λ6548	2.2 $\pm$ 0.1
Hα	84.5 $\pm$ 0.1
[N II] λ6584	6.33 $\pm$ 0.06
[S II] λ6717	7.46 $\pm$ 0.06
[S II] λ6731	5.59 $\pm$ 0.06

Notes. All fluxes have been measured from our Gemini spectrum. No reddening correction has been applied. There is an additional systematic uncertainty in the flux measurements of $\sim$10% due to flux calibration.

galaxy spectral components are shown in Figure 3. As illustrated in the figure, the broad, highly blended spectral features of SN 2010ay resemble those of the Type Ic-BL SN 2010bh (associated with GRB 100316D) at a similar epoch (Chornock et al. 2010). In particular, the broadening and blueshift of the feature near 6355 Å are similar for SN 2010ay and SN 2010bh and are broader and more blueshifted than in SN 1998bw at a comparable epoch. We discuss the comparison between these two SNe further in Sections 3.3 and 6.2.

Additionally, we obtained 60 s gri-band images of SN 2010ay on 2010 April 11.4 UT using GMOS. The data were reduced using the gemini package in IRAF, and photometry was performed using the standard GMOS zero points.[22] We measure that $[g, r, i] = [18.90, 18.32, 18.04] \pm 0.1$ mag.

Imaging photometry is not available at the epoch of our WHT spectrum. However, the spectrum was flux-calibrated against observations of the standard star Feige 34, which was observed the same night and at approximately the same low airmass as the SN. For the observations of both the standard star and SN, the slit was placed at the parallactic angle. We perform synthetic photometry on the spectrum to extract the flux at the central frequency of the R band (6527 Å) and find $R = 18.2 \pm 0.2$ mag. We then subtract the host galaxy flux numerically.

2.3.1. Host Galaxy Features

We measure fluxes of the narrow emission lines from the host galaxy in our Gemini spectrum, as reported in Table 3. We fit a Gaussian profile to each narrow emission line; for nearby lines such as [N II] and Hα, we fit multiple Gaussians simultaneously. We model the local continuum with a linear fit to 20 Å regions on either side of each line. We estimate uncertainties in quantities derived from the line fluxes by Monte Carlo propagation of the uncertainties in the flux measurement.

The host galaxy is significantly reddened as evidenced by the flux ratio of Hα to Hβ, $\approx 3.45 \pm 0.02$. We infer $E(B - V) = 0.2$ mag ($A_V = 0.6$ mag), as measured from the Balmer decrement in our Gemini spectrum, assuming $R_V = 3.1$, Case B recombination (Osterbrock & Ferland 2006), and the reddening law of Cardelli et al. (1989). This is similar to the value derived

---

[21] IRAF is distributed by the National Optical Astronomy Observatory, which is operated by the Association of Universities for Research in Astronomy (AURA) under cooperative agreement with the National Science Foundation.
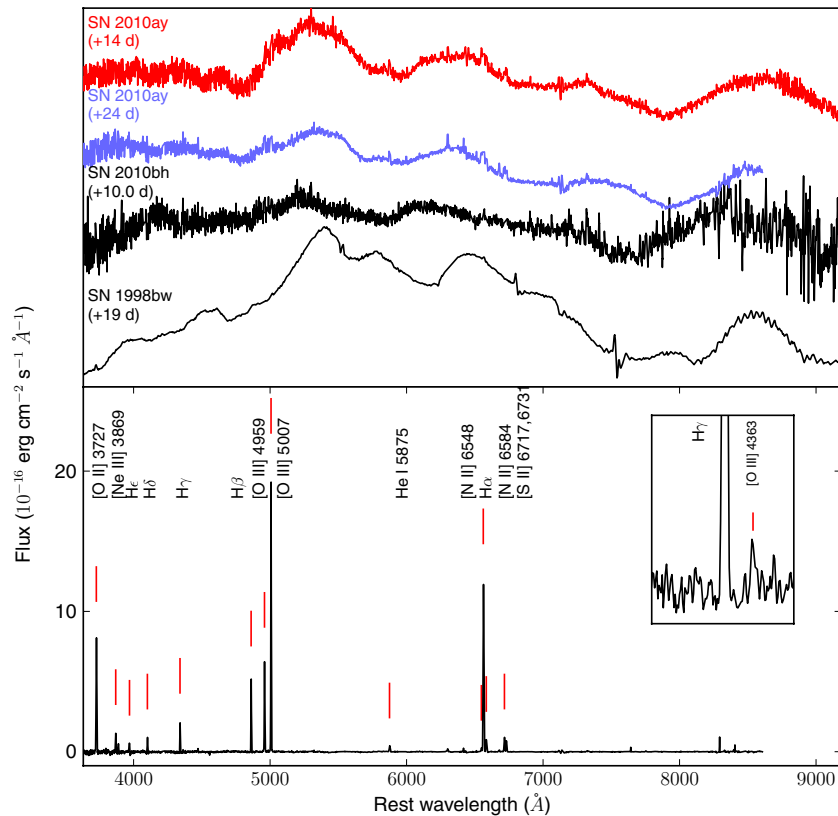
[22] http://www.gemini.edu/?q=node/10445

Figure 3. Optical spectra of SN 2010ay from Gemini (24 days after R-band peak) and the WHT (14 days). The spectrum is plotted decomposed into SN (above, with narrow lines clipped) and host galaxy (below, from Gemini, with spline-fit subtracted) components for clarity. The spectrum of SN 2010bh from Chornock et al. (2010) is given in black for comparison, at 21.2 days after the GRB 100316D trigger ($\sim$10.0 days after R-band peak; Cano et al. 2011a). The spectrum of SN 1998bw at +19 days from Patat et al. (2001) is also plotted. Both are transformed to the redshift of SN 2010ay. The SNe are shifted in flux for clarity. In the lower plot, relevant host galaxy emission lines are marked with a red line and labeled.

(A color version of this figure is available in the online journal.)

from the SDSS DR8 nuclear fiber spectroscopy line fluxes for the host galaxy ($E(B - V) = 0.2$ mag). The value reported in Modjaz et al. (2010) was also similar: $E(B - V) = 0.3$ mag. Furthermore, we note that the color ($B - V = 0.78 \pm 0.07$ mag) as reported by Prieto (2010) at 4 days after R-band peak is significantly redder than SN Ib/c color curve templates (Drout et al. 2011), further supporting a non-negligible host galaxy extinction.

2.4. Radio Observations

We observed SN 2010ay with the EVLA (Perley et al. 2009) on three epochs, 2010 March 26, 2010 April 29, and 2011 May 7. All EVLA observations were obtained with a bandwidth of 256 MHz centered at 4.9 GHz. We used calibrator J1221+2813 to monitor the phase and 3C 286 for flux calibration. Data were reduced using the standard packages of the Astronomical Image Processing System. We do not detect a radio counterpart to SN 2010ay in these observations and place upper limits of $F_\nu \lesssim 46, 42, 30\ \mu$Jy ($3\sigma$) for each epoch, respectively, corresponding to upper limits on the spectral luminosity spanning $L_\nu \lesssim (3.6\text{–}5.5) \times 10^{27}$ erg cm^{-2} s^{-1}.

As shown in Figure 4, these limits are comparable to the peak luminosities observed for ordinary SNe Ib/c (Berger et al. 2003a; Soderberg 2007; Chevalier & Fransson 2006; Soderberg et al. 2010, and references within) and a factor of $10^2\text{–}10^3$ less luminous than the radio afterglows associated with GRBs 020903, 030329, and 031203 at early epochs (Berger et al. 2003b; Soderberg et al. 2004a, 2004b; Frail

et al. 2005). In comparison with the radio luminosities observed for the relativistic SNe 1998bw (Kulkarni et al. 1998) and 2009bb (Soderberg et al. 2010), SN 2010ay is a factor of $\gtrsim$10 less luminous. The peak radio luminosity observed for GRB 100316D was a factor of a few higher than the first EVLA non-detection of SN 2010ay (E. Margutti et al. 2012, in preparation). The only relativistic explosion with detected radio emission below our EVLA limits is the weak and fast-fading XRF 060218 (Soderberg et al. 2006a).

3. INITIAL CONSTRAINTS

3.1. Light-curve Modeling

We construct an R-band light curve for SN 2010ay using the observations described in Section 2.3 (Table 2). We convert the i_{P1}- and r'-band data points to the R band using the fiducial light-curve method of Soderberg et al. (2006b), assuming the unextincted $i' - R$ and $r' - R$ colors observed for the Type Ic-BL SN 1998bw at the appropriate epoch (Galama et al. 1998). Photometry for the unfiltered CRTS images was reported by Drake et al. (2010) after transformation to the synthetic V band (A. J. Drake 2011, private communication); we therefore convert to the R band assuming the $V - R$ color of SN 1998bw at the appropriate epoch. For the Pan-STARRS1 photometry, the host galaxy flux was subtracted using a template image. For all other photometry, we have subtracted the flux of the host galaxy numerically assuming the magnitude reported in Table 1. A total
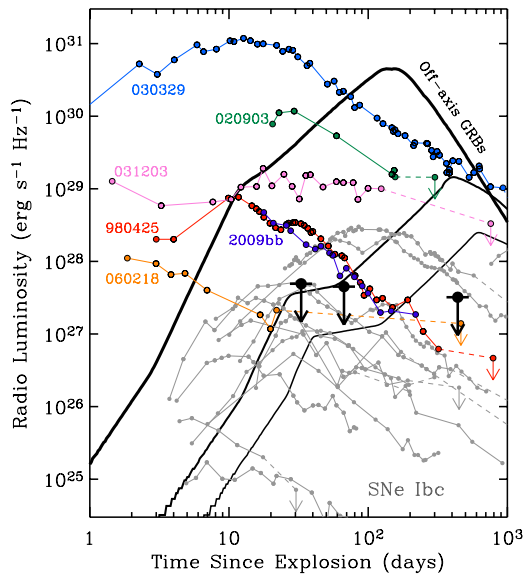
Figure 4. EVLA upper limits for SN 2010ay (black arrows) are compared with off-axis GRB afterglow light-curve models (black curves; standard parameters: $E_K \approx 10^{51}$ erg, $A_* = 1$, $\epsilon_e = \epsilon_B = 0.1$, $\theta_j = 5°$, and viewing angles of 30°, 60°, 90°) and the observed radio light curves for ordinary SNe Ib/c (gray; Soderberg 2007, and references within) and the radio afterglows of all GRB–SNe within $z \leqslant 0.25$. SN 2010ay is a factor of 10^2–10^3 less luminous than XRF 020903 (orange; Soderberg et al. 2004a), GRB 030329 (blue; Berger et al. 2003b; Frail et al. 2005), and GRB 031203 (Soderberg et al. 2004b). Relativistic, engine-driven SNe 1998bw (red; Kulkarni et al. 1998) and 2009bb (dark blue; Soderberg et al. 2010) are a factor of 10 more luminous than the SN 2010ay limits on a comparable timescale, while XRF 060218 lies a factor of a few below the limits. We constrain the radio counterpart to be no more luminous than XRF 060218 and comparable to the peak luminosities of ordinary SNe Ib/c.

(A color version of this figure is available in the online journal.)

(Galactic + host) reddening of $E(B - V) = 0.2$ mag has been assumed (see Section 2.3.1).

To estimate the explosion date of SN 2010ay, we have fit an expanding fireball model to the optical light curve (Figure 2), following Conley et al. (2006). In this model, the luminosity increases as

$$L \propto \left(\frac{t - t_0}{1 + z} \right)^n. \tag{1}$$

We derive an explosion date t_0 of 2010 February 21.3 ± 1.3. Here, we have assumed an index $n = 2$. This suggests that the PS1 3π i_{P1}-band pre-discovery detection image of SN 2010ay was taken ~4 days after the explosion. Observations by the PS1 survey have therefore provided a valuable data point for estimating the explosion date and also for constraining the rise time of SN 2010ay, as well as other nearby SNe (e.g., SN 2011bm; Valenti et al. 2012).

In Figure 2, we compare the light curve of SN 2010ay to the SN Ib/c light-curve template of Drout et al. (2011) after stretching by a factor of $(1 + z)$. The template provides a reasonable fit to the optical evolution of SN 2010ay. Fitting the template to our photometry, we derive (reduced $\chi^2 = 0.3$) a date of R-band peak of 2010 March 18 ± 2 UT (MJD 55,273 ± 2) and an R-band peak magnitude of $M_R \approx -19.7$ mag before extinction correction. As discussed in Section 2.3.1, based on the Balmer decrement observed for the host galaxy emission lines, we assume an extinction of $E(B - V) = 0.2$ mag. Applying this correction, the peak absolute magnitude is $M_R \approx -20.2 \pm 0.2$ mag. We note that this fitted value is ≈0.2 mag

fainter than that estimated from the data point near peak. Here, the uncertainty is dominated by the template fitting.

Regardless of the extinction correction, SN 2010ay is more luminous than all the 25 SNe Ib/c in the sample of Drout et al. (2011), except for SN 2007D ($M_R \approx -20.65$ mag, which was also significantly extincted: $A_V \sim 1.0$ mag). Assuming an intrinsic $V - R$ color of zero at peak (e.g., 1998bw: Galama et al. 1998; Patat et al. 2001), SN 2010ay is also more luminous than any of the 22 GRB and XRF-producing SNe in the compilation of Cano et al. (2011b), all corrected for extinction, and is 1.5 standard deviations from the mean luminosity. The peak magnitude is only ~1 mag below that of the Type Ic SN 2007bi ($M_R = -21.3 \pm 0.1$ mag), which Gal-Yam et al. (2009) report as a candidate pair-instability SN.

3.2. Large Nickel Mass for SN 2010ay

We use the available photometry for SN 2010ay discussed above to derive the mass of ^{56}Ni required to power the optical light curve under the assumption that the emission is powered by radioactive decay. Using the relation between M_{Ni} and M_R found by Drout et al. (2011), $\log(M_{Ni}) = (-0.41 M_R - 8.3) M_\odot$, we estimate that SN 2010ay synthesized a nickel mass of $M_{Ni} = 0.9^{+0.1}_{-0.1} M_\odot$. We have estimated the uncertainty in the M_{Ni} estimate by propagation of the uncertainty in the template fitted peak magnitude—systematic uncertainties are not included. If we instead adopt the most luminous individual data point in the light curve as the peak value, rather than the smaller peak value from template fitting, we find $M_{Ni} \approx 1.2 M_\odot$.

The M_{Ni} estimate for SN 2010ay is larger than that of all but one (SN 2007D) of the 25 SNe Ib/c in the Drout et al. (2011) compilation and significantly larger than the estimate for GRB–SN 2010bh, $M_{Ni} = 0.12 \pm 0.01 M_\odot$ (Cano et al. 2011a). On the other hand, M_{Ni} of SN 2010ay is at least 3 times smaller than for SN 2007bi ($M_{Ni} \approx 3.5$–4.5 $M_\odot$; Young et al. 2010). A pair-instability SN should produce $M_{Ni} \gtrsim 3 M_\odot$ (Gal-Yam et al. 2009).

3.3. Unusually High Velocity

As illustrated in Figure 3, the broad, highly blended spectral features of SN 2010ay at the time of the WHT observations (14 days after R-band peak; see Section 3.1) resemble those of SN 2010bh at a similar time (10.0 days after peak; Chornock et al. 2010). In particular, the blueshift of the feature near 6355 Å is larger than in SN 1998bw and more similar to SN 2010bh. This feature is commonly associated with Si II λ6355 (e.g., Patat et al. 2001). However, this feature has two clearly detectable absorption minima in SN 2010ay, but not in SN 2010bh. This could be due to increased blending in SN 2010bh or the absence of contaminating lines. The red ends of the SN 2010ay and SN 2010bh spectra (rest wavelength > 7500 Å) have similar P Cygni features, but the emission and absorption components in SN 2010bh are each blueshifted by ~200 Å more than in the spectrum of SN 2010ay. Chornock et al. (2010) attribute this feature to the Ca II near-IR (NIR) triplet, with a gf-weighted line centroid of 8479 Å, and find a velocity that is high but consistent with the early-time velocity of Si II λ6355 ($(30$–$35) \times 10^3$ km s^{-1}).

We measure the absorption velocity from the minimum of the Si II λ6355 absorption feature (v_{Si}). We smooth the spectrum using an inverse-variance-weighted Gaussian filter (Blondin et al. 2006, with $d\lambda/\lambda = 0.005$) and measure the minimum position of the redmost component of the absorption profile.
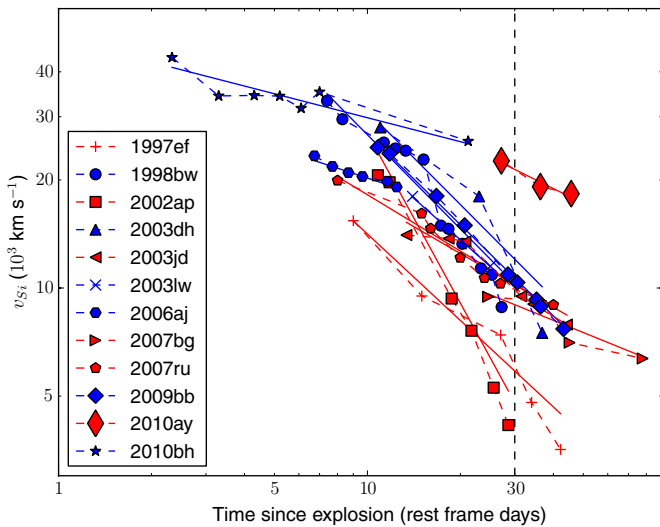
Figure 5. Comparison of the time-evolving absorption velocity of SN 2010ay and other SNe Ic-BL (red) and engine-driven explosions (blue) from the literature. For each SN, we fit a power law of the form $v_{Si} = v_{Si}^{30}(t/30)^{\alpha}$, where t is the time in days, v_{Si}^{30} is the velocity at 30 days after explosion (dashed vertical line), and α is the velocity gradient. The velocities for SNe 1997ef, 2003dh, and 2003lw are from Mazzali et al. (2006), as determined by spectral modeling. The velocities for all other SNe are measured from the Si II $\lambda6355$ feature as follows: SN 2007ru is from Sahu et al. (2009); SNe 1998bw, 2006aj, and 2010bh are from Chornock et al. (2010), from spectra in references therein; SN 2007bg is from Young et al. (2010); SNe 2002ap, 2009bb, and 2003jd are from Pignata et al. (2011), and references therein; and SN 2010ay is from Prieto (2010) and this paper. See Table 4 for uncertainties.

(A color version of this figure is available in the online journal.)

Table 4
Velocity Evolution of SNe Ic-BL

SN	v_{Si}^{30}	α
SNe Ic-BL		
1997ef	6 ± 2	-0.8 ± 0.4
2002ap	5 ± 2	-1.5 ± 0.7
2003jd	10 ± 1	-0.5 ± 0.2
2007bg	9 ± 2	-0.3 ± 0.2
2007ru	10.3 ± 0.7	-0.5 ± 0.1
2010ay	21 ± 2	-0.4 ± 0.3
Engine-driven SNe Ic-BL		
1998bw	10.3 ± 0.7	-0.86 ± 0.08
2003dh	12.0 ± 0.9	-0.9 ± 0.1
2003lw	10 ± 1	-0.8 ± 0.2
2006aj	15 ± 3	-0.3 ± 0.2
2009bb	10.7 ± 0.4	-0.84 ± 0.08
2010bh	24 ± 3	-0.22 ± 0.07

Notes. To the velocity measurements for each SN, we have fit a power law of the form $v_{Si} = v_{Si}^{30}(t/30)^{\alpha}$, where t is the time since explosion in days and v_{Si}^{30} is the velocity at 30 days in units of 10^3 km s^{-1}. These power-law fits are illustrated in Figure 5. We adopt a conservative error of 10% on individual velocity measurements in order to compare the allowable range of fitted parameters for different SNe and note that this uncertainty is likely dominated by systematic effects. Uncertainties in the explosion date for SNe without detected GRBs vary due to availability of early-time photometry; we adopt the following conservative uncertainties: 7 days (1997ef; Hu et al. 1997), 7 days (2002ap; Gal-Yam et al. 2002), 6 days (2003jd; Valenti et al. 2008), 14 days (2007bg), 3 days (2007ru; Sahu et al. 2009), 1 day (2009bb; Pignata et al. 2011), and 2 days (2010ay; this paper).

The blue component of the absorption profile shifts blueward over time, suggesting that it is produced by a combination of ions separated by several 10^3 km s^{-1}, such as He I $\lambda5876$ and Na I D, whose relative optical depth changes with time.

The absorption velocity inferred from the Si II $\lambda6355$ feature is ~2 times faster than that of SN 1998bw at similar times, and more similar to that of SN 2010bh (Figure 3). For SN 1998bw, Patat et al. (2001) measured $\sim10 \times 10^3$ km s^{-1} at +13 days. For SN 2010bh, Chornock et al. (2010) measured $v_{Si} \approx 26 \times 10^3$ km s^{-1} at +10.0 days after explosion. Prieto (2010) reported a velocity of $v_{Si} \approx 22.6 \times 10^3$ km s^{-1} from the Si II $\lambda6355$ feature in a spectrum of SN 2010ay taken at +4 days; Prieto (2010) does not discuss the details of their methodology for the velocity measurement. From our [WHT, Gemini] spectra taken [+14, +24] days after R-band peak (see Section 3.1), we estimate $v_{Si} \approx [19.2, 18.3] \times 10^3$ km s^{-1}.

In addition to the broadening of the spectral features and the blueshift of the Si II $\lambda6355$ line, additional lines of evidence suggest a high photospheric expansion velocity for SN 2010ay. We measure $v_{Si} \approx [21.7, 20.1] \times 10^3$ km s^{-1} from the Ca II NIR triplet on the smoothed [WHT, Gemini] spectra, relative to a line center at 8479 Å. This is within a few $\times 10^3$ km s^{-1} of the v_{Si} we measure from Si II $\lambda6355$ at these epochs. Furthermore, we do not detect the broad emission "bump" near 4500 Å in either of our spectra. This feature was also absent in SN 2010bh but was identified in SN 2003dh, SN 2006aj, and several Ic-BLs not associated with GRBs and normal SNe Ic; Chornock et al. (2010) suggest that the absence of this feature indicates a high expansion velocity if it is due to blending of the iron lines to the blue and red of 4500 Å.

We compare the late-time expansion velocity of SN 2010ay to other SNe Ic-BL and GRB–SNe with detailed, multi-epoch

velocity measurements from the literature in Figure 5. We note that the velocities for SNe 1997ef, 2003dh, and 2003lw plotted in the figure were estimated by Mazzali et al. (2006) via spectral modeling, rather than measured directly from the minimum of the Si II $\lambda6355$ absorption feature; however, these velocities should be equivalent to within a few 10^3 km s^{-1}, as the minimum of the Si II feature is typically well fit by the photospheric velocity of the spectral models (see, e.g., Mazzali et al. 2000; Kinugasa et al. 2002). In this figure, we also fit power-law gradients to the time evolution of the velocity of these SNe with the form $v_{Si} = v_{Si}^{30}(t/30)^{\alpha}$, where t is the time since explosion in days and v_{Si}^{30} is the velocity at 30 days in units of 10^3 km s^{-1}. These parameters are listed in Table 4. Figure 5 illustrates that most SNe are well described by a single power law.[23] However, due to lack of late-time spectroscopy, the v_{Si}^{30} measurement amounts to an extrapolation for some objects (particularly 2006aj), and contamination from different ions or detached features will add uncertainty to velocities measured from the Si II $\lambda6355$ feature.

SNe 2010ay and 2010bh share high characteristic velocities at 30 days after explosion and velocity gradients that are low relative to other broad-lined SNe Ic with and without associated GRBs. For SN 2010ay, $v_{Si}^{30} = 21 \pm 2$ is 2–4 times larger than for other SNe Ic-BL without associated GRBs ($v_{Si}^{30} = 6 \pm 2$ for 1997ef, 5 ± 2 for 2002ap, 10 ± 1 for 2003jd, 9 ± 2 for 2007bg, and 10.3 ± 0.7 for 2007ru) and is similar to the GRB–SN 2010bh ($v_{Si}^{30} = 24 \pm 3$). No other GRB–SN or SN Ic-BL has $v_{Si}^{30} > 15$. The SNe Ic-BL and GRB–SNe with the

---

[23] A break at $\sim2 \times 10^4$ km s^{-1} appears to exist for SN 1998bw at ~16 days, as noted by Kinugasa et al. (2002).

most shallow velocity gradients among these 12 objects have $\alpha < -0.5$; they are SN 2006aj ($\alpha = -0.3 \pm 0.2$), SN 2007bg ($\alpha = -0.3 \pm 0.2$), SN 2010ay ($\alpha = -0.4 \pm 0.3$), and SN 2010bh ($\alpha = -0.22 \pm 0.07$). This places SN 2010ay in the company of two GRB–SNe in having a slowly evolving absorption velocity and SN 2007bg (whose unusually fast decline rate distinguishes it from other SNe Ic-BL; Young et al. 2010). The velocities of SNe 2010ay and 2010bh, respectively, decline about 2 and 4 times more slowly than the other SNe Ic-BL (mean and standard deviation: $\alpha = -0.8 \pm 0.4$) and about 1.5 and 3 times more slowly than the other GRB–SNe ($\alpha = -0.7 \pm 0.2$). The slow Si II $\lambda6355$ absorption velocity evolution of SN 2010ay at late times resembles the slow evolution of the Fe II lines of the spectroscopically normal Type Ic SNe 2007gr and 2011bm at late times (Valenti et al. 2012).

Given the high peak luminosity of SN 2010ay (Section 3.1), we also consider the velocity of the candidate pair-instability SN 2007bi. Velocity measurements for SN 2007bi are only available at late times (>50 days; Young et al. 2010). Fitting to these late-time Si II $\lambda6355$ velocity measurements, we find that SN 2007bi has a characteristic velocity ~3 times smaller than 2010ay ($v_{Si}^{30} = 8 \pm 2$) and the late-time velocity gradient is ~2 times more shallow ($\alpha = -0.2 \pm 0.2$).

3.4. Ejecta Mass and Energy

We use the scaling relations provided by Drout et al. (2011), based on the original formalism of Arnett (1982) and modified by Valenti et al. (2008), to derive the total mass of the ejecta and the kinetic energy

$$M_{ej} = 0.8 \left(\frac{\tau_c}{8\,\mathrm{d}} \right)^2 \left(\frac{v_{Si}}{10{,}000\,\mathrm{km\,s^{-1}}} \right) M_\odot \qquad (2)$$

$$E_K = 0.5 \left(\frac{\tau_c}{8\,\mathrm{d}} \right)^2 \left(\frac{v_{Si}}{10{,}000\,\mathrm{km\,s^{-1}}} \right)^3 \times 10^{51}\,\mathrm{erg}. \qquad (3)$$

We assume the fitted peak magnitude for SN 2010ay ($M_R = -20.2 \pm 0.2$; Section 3.1), the absorption velocity we measure from our WHT spectrum at 14 days after maximum light ($v_{Si} = 19.2 \times 10^3\,\mathrm{km\,s^{-1}}$; Section 3.3), and a characteristic time (light-curve width) consistent with the data and the mean value from the Drout et al. (2011) sample of SNe Ic-BL ($\tau_c = 14$ days).

Using these values, the total mass ejected was $M_{ej} \approx 4.7\,M_\odot$, and the total kinetic energy of the explosion was $E_K \approx 10.8 \times 10^{51}$ erg. Hereafter we refer to the definition $E_{K,51} = E_K / 10^{51}$ erg.

The systematic uncertainties associated with this modeling dominate the statistical uncertainties. In particular, the models rely on the assumptions of homologous expansion, spherical symmetry, all ^{56}Ni centralized at the center of the ejecta, optically thick ejecta, and constant opacity.

We note that an earlier measurement of the absorption velocity is preferred for optical modeling. Since we have argued that SN 2010ay and SN 2010bh have similar characteristic velocities (v_{Si}^{30}), if we instead adopt a higher velocity of 25,000 km s^{-1} as measured for SN 2010bh by Cano et al. (2011a), we estimate $M_{ej} \approx 6.1\,M_\odot$ and $E_{K,51} \approx 23.9$ for SN 2010ay.

The M_{ej} and $E_{K,51}$ of SN 2010ay are consistent with the mean for SNe Ic-BL in the Drout et al. (2011) sample ($4.7^{+2.3}_{-1.8}\,M_\odot$ and 11^{+6}_{-4}, respectively), because the authors assumed a velocity ($v_{Si} = 2 \times 10^4\,\mathrm{km\,s^{-1}}$) similar to the late-time velocity we measure. For comparison, SN 2010bh had a total ejecta mass of

$\sim2\,M_\odot$ and a total kinetic energy of $E_{K,51} \approx 13$ (Cano et al. 2011a).

The ratio of Ni to total ejecta mass is ~0.2 for SN 2010ay, significantly higher than the values typical of SNe Ic-BL and GRB–SNe. For comparison, the ratio is just ~0.05 for SN 2010bh. Adopting the values derived from bolometric light-curve modeling by Cano et al. (2011a), the M_{Ni} and M_{Ni}/M_{ej} ratios for other GRB–SNe are $\sim0.5\,M_\odot$ and ~0.06–0.22 (1998bw), $\sim0.4\,M_\odot$ and ~0.08 (2003dh), $\sim0.15\,M_\odot$ and ~0.07–0.1 (2006aj), and $\sim0.2\,M_\odot$ and ~0.06 (2009bb). This ratio for SN 2010ay is larger than that of all but 4 of the 25 SNe of Drout et al. (2011): the Type Ic SNe 2004ge ($M_{Ni}/M_{ej} \sim 0.4$) and 2005eo ($M_{Ni}/M_{ej} \sim 0.2$), the Type Ib SN 2005hg (~0.4), and the Type Ic-BL SN 2007D (~0.6).

The large value of M_{Ni} we estimate for SN 2010ay raises the question of whether a process other than Ni decay may be powering its light curve (e.g., Chatzopoulos et al. 2009). An independent test of the physical process powering the light curve is the decay rate of the late-time light curve, which should be ≈0.01 mag day^{-1} for SNe powered by radioactive decay of ^{56}Co. For SN 2007bi, Gal-Yam et al. (2009) derive $M_{Ni} = 3.5\,M_\odot$ from the measured peak magnitude and find that the late-time light curve is consistent with the decay rate of ^{56}Co. While the Pan-STARRS1 3π survey also observed the field in 2011 March, the SN was not detected in our subtracted images, and the limits are not constraining in the context of ^{56}Co decay (see Section 2.2 and Table 2). Another possible process is a radiation-dominated shock that emerges due to interaction with an opaque circumstellar medium (CSM), as has recently been proposed by Chevalier & Irwin (2011) for the ultraluminous SNe 2006gy and 2010gx (Pastorello et al. 2010; Quimby et al. 2011). However, while this class of ultraluminous objects shares some spectroscopic similarities to SNe Ic (Pastorello et al. 2010), they show peak luminosities ~4–100 times higher than SN 2010ay (Chomiuk et al. 2011; Quimby et al. 2011).

4. CONSTRAINTS ON RELATIVISTIC EJECTA

We use our EVLA upper limits for SN 2010ay spanning $\Delta t \approx 29$–433 days to constrain the properties of the shock wave and those of the local circumstellar environment. The radio emission from SNe Ib/c and GRBs is produced by the dynamical interaction of the fastest ejecta with the surrounding material (Chevalier 1982). The kinetic energy of the ejecta is converted, in part, to internal energy of the shocked material, which itself is partitioned between relativistic electrons (ϵ_e) and amplified magnetic fields (ϵ_B). Following the breakout of the shock wave from the stellar surface, electrons in the environment of the explosion are shock-accelerated to relativistic velocities with Lorentz factor γ_e and distributed in a power-law distribution characterized by $N(\gamma_e) \propto \gamma_e^{-p}$. Here, p characterizes the electron energy index. The particles gyrate in amplified magnetic fields and give rise to non-thermal synchrotron emission that peaks in the radio and mm-bands in the days to weeks following explosion with observed spectral index $F_\nu \propto \nu^{-(p-1)/2}$. At lower frequencies the emission is suppressed due to synchrotron self-absorption, which defines a spectral peak, ν_p (Chevalier 1998).

The dynamics of the shock wave determine the evolution of the synchrotron spectrum and, in turn, the properties of the observed radio light curves. In the case of SNe Ib/c, there are three primary scenarios for the dynamical regime of the ejecta depending on the shock velocity, $v = \beta c$ (associated Lorentz

factor, Γ): (1) non-relativistic ($v \approx 0.2c$) free expansion as in the case of ordinary SNe Ib/c (Chevalier 1998); (2) a decoupled and relativistic ($\Gamma \sim 10$) shell of ejecta that evolves according to the Blandford–McKee solution for several months (Sari et al. 1998) before transitioning to the Sedov–Taylor regime (Frail et al. 2000; this is the standard scenario for typical GRBs); and (3) a sub-energetic GRB with trans-relativistic velocity ($\beta\Gamma \lesssim 3$) that bridges the free-expansion and Blandford–McKee dynamical regimes (e.g., SN 1998bw; Kulkarni et al. 1998; Li & Chevalier 1999).

We consider our EVLA upper limits in the context of these three models below. For shock velocities of $v \gtrsim 0.2c$, $\epsilon_e \approx 0.1$ is reasonable (Soderberg et al. 2005; Chevalier & Fransson 2006). We further assume equipartition, $\epsilon_e = \epsilon_B = 0.1$. We adopt a free-expansion model for both the non-relativistic ordinary SN Ib/c case and the sub-energetic, trans-relativistic GRB scenario. As shown by Li & Chevalier (1999), a free-expansion model is still reasonable in the trans-relativistic regime (case 3, see above).

4.1. Freely Expanding Shock Wave

In the free-expansion scenario, a shock discontinuity separates the forward and reverse shocks, located at the outer edge of the stellar envelope. The bulk ejecta is in free expansion, while the thin layer of post-shock material is slightly decelerated, $R \propto t^{0.9}$ (Chevalier & Fransson 2006). At a given frequency, the bell-shaped light curves of the SN synchrotron emission may be described as (Chevalier 1998)

$$L_\nu \approx 1.582 \times L_{\nu,p}\left(\frac{\Delta t}{t_p}\right)^a [1 - e^{-(\Delta t/t_p)^{-(a+b)}}], \qquad (4)$$

where $L_{\nu,p}$ is the flux density at the spectral peak at epoch t_p. Assuming an electron index of $p \approx 3$, consistent with radio spectra of SNe Ib/c (Chevalier & Fransson 2006), the exponents are $a \approx 2.3$ and $b \approx 1.3$. The time-averaged shock wave velocity is $\bar{v} \approx R/\Delta t$, where R is the shock wave radius defined as

$$R \approx 2.9 \times 10^{16}\left(\frac{\epsilon_e}{\epsilon_B}\right)^{-1/19}\left(\frac{L_{\nu,p}}{10^{28}\,\mathrm{erg\,s^{-1}\,Hz^{-1}}}\right)^{9/19}$$
$$\times \left(\frac{\nu_p}{5\,\mathrm{GHz}}\right)^{-1}\,\mathrm{cm}. \qquad (5)$$

Here, we make the assumption that the radio-emitting region is half of the total volume enclosed by a spherical blast wave. Next, we estimate the internal energy, E, of the radio-emitting material from the post-shock magnetic energy density, $E \approx B^2 R^3/12\epsilon_B$, where we maintain the assumption of equipartition. As shown by Chevalier (1998), the amplified magnetic field at peak luminosity is also directly determined from the observed radio properties,

$$B \approx 0.43\left(\frac{\epsilon_e}{\epsilon_B}\right)^{-4/19}\left(\frac{L_{\nu,p}}{10^{28}\,\mathrm{erg\,s^{-1}\,Hz^{-1}}}\right)^{-2/19}$$
$$\times \left(\frac{\nu_p}{5\,\mathrm{GHz}}\right)\,\mathrm{G}. \qquad (6)$$

Finally, the mass-loss rate of the progenitor star, $\dot{M}$, may be derived from the number density of emitting electrons. Here, we normalize the wind profile according to $\rho \propto Ar^{-2}$ and $A_* = A/5 \times 10^{11}\,\mathrm{g\,cm^-}$. This normalization of A_* implies that an A_* of 1 corresponds to typical Wolf–Rayet progenitor wind
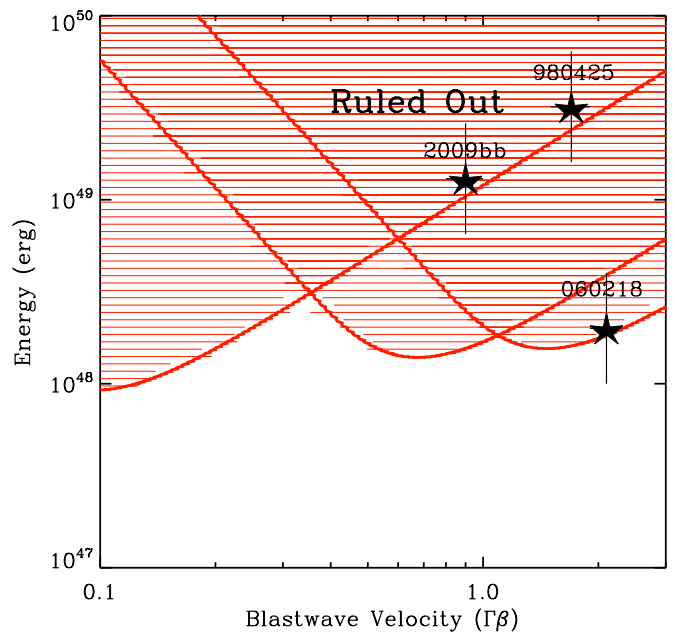

Figure 6. Region of energy–velocity space ruled out (red) by our EVLA observations for on-axis ejecta under the assumption of a free-expansion model.
(A color version of this figure is available in the online journal.)

properties of $\dot{M} = 10^{-5}\,M_\odot\,\mathrm{yr^{-1}}$ and a progenitor wind velocity of $v_w = 10^3\,\mathrm{km\,s^{-1}}$:

$$A_* \approx 0.15\left(\frac{\epsilon_B}{0.1}\right)^{-1}\left(\frac{\epsilon_e}{\epsilon_B}\right)^{-8/19}\left(\frac{L_{\nu,p}}{10^{28}\,\mathrm{erg\,s^{-1}\,Hz^{-1}}}\right)^{-4/19}$$
$$\times \left(\frac{\nu_p}{5\,\mathrm{GHz}}\right)^2\left(\frac{\Delta t}{10\,\mathrm{days}}\right)^2\,\mathrm{cm^{-1}}, \qquad (7)$$

where we assume a shock compression factor of ~ 4 and a nucleon-to-electron ratio of 2.

We built a two-dimensional grid of fiducial radio light curves according to Equation (4) in which we vary the parameters L_{ν_p} and ν_p over a reasonable range of parameter space, bounded by $t_p \approx [1, 3000]$ days and $F_{\nu,p} \approx 0.04$–1000 mJy. We identify the fiducial light curves associated with a radio luminosity *higher* than the EVLA upper limits for SN 2010ay at each epoch as these are excluded by our observations. We extract the physical parameters associated with these excluded light curves (R, B, E, A_*) to define the parameter space excluded by our radio observations. The parameter space for ν_p and $F_{\nu,p}$ is bounded by the respective values for which the model exceeds relativistic velocities, $\beta\Gamma \sim$ few.

As shown in Figure 6, our deep EVLA limits enable us to rule out a scenario in which there is copious energy, $E \gtrsim 10^{48}$ erg, coupled to a relativistic outflow, in this two-dimensional $E - v$ parameter space. The excluded region includes GRB–SNe 1998bw and 060218, as well as the relativistic SN 2009bb. It does not exclude the standard scenario in which a small percent of the energy is coupled to fast-moving material within the homologous outflow, as is typically observed for ordinary SNe Ib/c ($E \approx 10^{47}$ and $v \approx 0.2c$; Soderberg et al. 2010).

Next we consider the effects of circumstellar density since lower mass-loss rates produce fainter radio counterparts. As shown in Figure 7, the EVLA limits for SN 2010ay exclude the region of parameter space populated by SNe 1998bw and
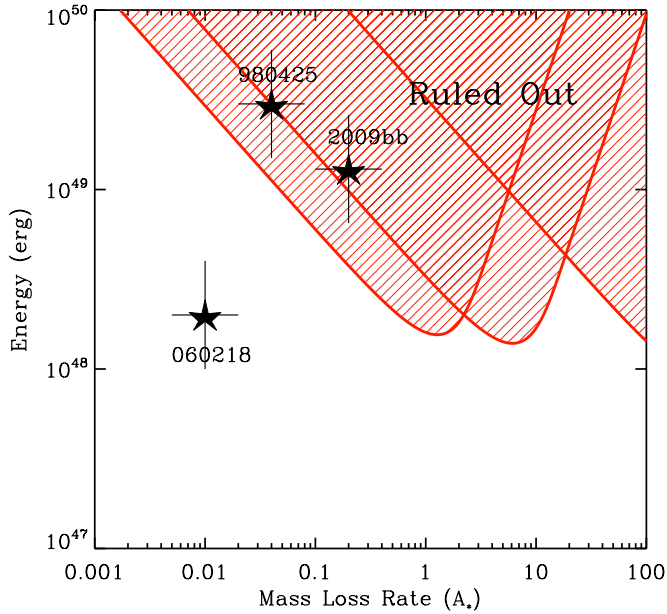
Figure 7. Region of energy–mass-loss space ruled out (red) by our EVLA observations for on-axis ejecta under the assumption of a free-expansion model.

(A color version of this figure is available in the online journal.)

Figure 8. Our EVLA observations at $\Delta t \approx 1.2$ years after explosion constrains the properties of a possibly associated off-axis GRB jet. Using our semianalytic model as described in Section 4.2, we assume partition fractions of $\epsilon_e = \epsilon_B = 0.1$, $\theta_j = 5°$, $p = 2.5$, and an off-axis viewing angle of $\theta_{oa} = 90°$. We are able to exclude the region of $E_K - A_*$ parameter space (red) associated with typical GRBs, i.e., $E_K = 10^{51}$ erg and $A_* = 1$ (dashed black lines).

(A color version of this figure is available in the online journal.)

2009bb with mass-loss rates of $A_* \sim 0.1$; however, the low-density environment of GRB 060218 lies outside of our excluded region due to its lower CSM density, $A_* \sim 0.01$, which gives rise to a lower luminosity radio counterpart.

4.2. Relativistic Ejecta

In the case of relativistic deceleration the ejecta are confined to a thin jet and are physically separated from the homologous SN component. Deceleration of the jet occurs on a timescale of $\Delta t \approx (E_{51}/A_*)$ years in a wind-stratified medium (Waxman 2004). On this same timescale, any ejecta components that were originally off-axis spread sideways into the observer's line of sight. While the early EVLA limits constrain the properties of the on-axis ejecta according to the free-expansion model described above, the late-time EVLA upper limits constrain any radio emission from a GRB jet originally pointed away from our line of sight.

For this scenario, we adopt the semianalytic model of Soderberg et al. (2006c) for off-axis GRB jets. In Figure 4, we compare the radio upper limits for SN 2010ay with the predictions for an off-axis jet with standard parameters ($E_K \approx 10^{51}$ erg, $A_* = 1$, $\epsilon_e = \epsilon_B = 0.1$, and $\theta_j = 5°$) and assuming a viewing angle of $\theta_{oa} = 30°, 60°$, or $90°$. Our EVLA upper limits rule out all three of these model light curves. We derive the two-dimensional parameter space (energy and CSM density) that is excluded based on our EVLA upper limit at $\Delta t \approx 1.2$ years. We note that this model accommodates the full transition from relativistic to non-relativistic evolution. We built a collection of model light curves spanning parameter range $A_* \approx [0.01–100]$ and $E \approx [10^{49}–10^{52}]$ erg, maintaining the assumption of $p = 3$ and $\epsilon_e = \epsilon_B = 0.1$. Here, we adopted a jet opening angle of $\theta_j = 5°$ and an off-axis viewing angle of $\theta_{oa} = 90°$ (the most conservative scenario). We note that van Eerten & MacFadyen (2011) have developed off-axis GRB afterglow light-curve models based on hydrodynamic simulations that reproduce the semianalytic models presented here to within factors of a few (see also van Eerten et al. 2010).
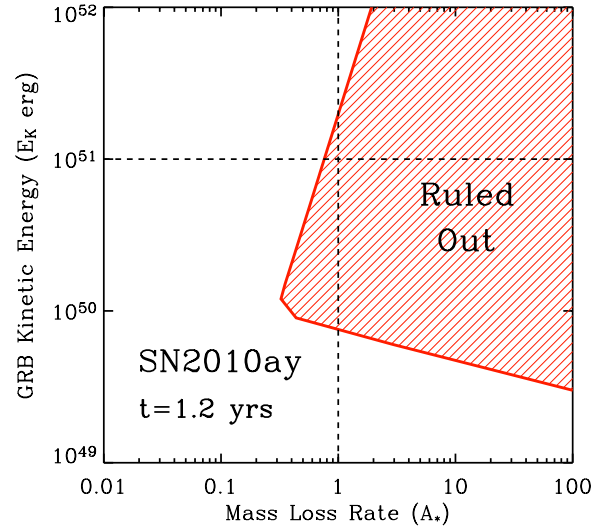
As shown in Figure 8, we are able to exclude the parameter space associated with typical GRBs, i.e., $E \approx 10^{51}$ erg (beaming corrected) and $A_* \approx 1$. GRBs with lower energies and densities are better constrained using the trans-relativistic formalism above. In conclusion, our radio follow-up of SN 2010ay reveals no evidence for a relativistic outflow similar to those observed in conjunction with the nearest GRB–SNe; however, a weak afterglow like that seen from XRF 060218 cannot be excluded.

5. CONSTRAINTS ON AN ASSOCIATED GRB

Given the estimate of the explosion date we have derived (Section 3.1), we have searched for gamma-ray emission that may have been detected by satellites. No GRBs consistent with SN 2010ay were reported in the circulars of the Gamma-ray Coordinates Network Circulars, but it is possible that bursts were detected below the instrument triggering thresholds.

We next consulted the sub-threshold bursts from the *Swift* Burst Alert Telescope (BAT; Gehrels et al. 2004; Barthelmy et al. 2005) detected within the 6 days surrounding the explosion date estimate. We find that no gamma-ray emission was detected within 0°.5 of the position of SN 2010ay by the BAT during this period. Given the sensitivity of the BAT, this corresponds to an upper limit on the gamma-ray flux of $\sim 10^{-8}$ erg s^{-1} cm^{-2} (15–150 keV). However, the field of SN 2010ay was in the field of view of the instrument for only 106 ks during these 6 days, or $\sim 20\%$ of the duration.

For complete temporal coverage, we have searched the records of the interplanetary network (IPN), which is sensitive to bursts with fluences down to $\sim 6 \times 10^{-7}$ erg cm^{-2} (25–150 keV) (50% efficiency limit; Hurley et al. 2010) and observes the entire sky with a temporal duty cycle close to 100%. An undetected, sub-threshold burst should have a fluence below this limit. Between 2010 February 21 and 25, inclusive, a total of 12 bursts were detected by the spacecraft of the IPN (Mars Odyssey, Konus-*Wind*, *RHESSI*, *INTEGRAL* (SPI-ACS), *Swift*-BAT, *Suzaku*, *AGILE*, MESSENGER, and *Fermi* (GBM)). Ten of them are confirmed bursts; they were observed by more than

one instrument on one or more spacecraft and could be localized. Two of them are unconfirmed bursts; they were observed by one instrument on one spacecraft (*Suzaku*). The total area of the localizations of the 10 confirmed bursts is $\sim 0.58 \times 4\pi$ sr. This implies that about 0.58 bursts can be expected to have positions that are consistent with any given point on the sky simply by chance (i.e., within the 3σ error region), and indeed *none* of the bursts in this sample have a position consistent with the SN position.

These non-detections imply upper limits to the gamma-ray energy (E_γ) of a burst that may have been associated with SN 2010ay. The IPN non-detection indicates $E_\gamma \lesssim 6 \times 10^{48}$ erg (25–150 keV), while the BAT non-detection indicates that the peak energy of the burst was $\lesssim 1 \times 10^{47}$ erg s^{-1} (15–150 keV) if the burst occurred while in the field of view of the instrument.

We consider whether or not a hypothetical GRB associated with SN 2010ay would have been detected by BAT or the IPN if it had characteristics similar to well-studied SN-associated GRBs. The isotropic prompt energy release of long GRBs is typically $E_{\gamma,\mathrm{iso}} \sim 10^{52}$ erg; however, the prompt emission of the sub-energetic class of GRB–SNe can be several orders of magnitude fainter (Soderberg et al. 2006a). GRB 980425/SN 1998bw had a peak gamma-ray luminosity of $\sim 5 \times 10^{46}$ erg s^{-1} (24–1820 keV; Galama et al. 1998), which is a factor of two below our BAT limit, and $E_{\gamma,\mathrm{iso}} \sim 5 \times 10^{47}$ erg (Pian et al. 2000), more than a factor of five below our limit. Neither satellite should have detected such a burst. In contrast, GRB 031203/SN 2003lw had a peak gamma-ray luminosity of $\sim 1 \times 10^{49}$ erg s^{-1} (20–200 keV) and a total isotropic equivalent energy of $E_{\gamma,\mathrm{iso}} = (4 \pm 1) \times 10^{49}$ erg (Sazonov et al. 2004), about two orders of magnitude above the sensitivity of the BAT and twice the threshold of the IPN, respectively. GRB 030329/2003dh was even more luminous, with $E_{\gamma,\mathrm{iso}} \sim 7 \times 10^{49}$ erg (Hjorth et al. 2003). A burst like GRB 031203 or 030329 should certainly have been detected by IPN, or the BAT if it occurred while the field of SN 2010ay was in the field of view of the instrument. XRF 060218/SN 2006aj, an extremely long duration ($\Delta t \approx 2000$ s) event, had a peak luminosity observed by BAT of $\sim 10^{-8}$ erg cm^{-2} s^{-1} (15–150 keV), corresponding to a peak emission of $\approx 2.4 \times 10^{46}$ erg s^{-1} given the redshift of the burst ($z = 0.033$), and a total isotropic equivalent energy of $E_{\gamma,\mathrm{iso}} = (6.2 \pm 0.3) \times 10^{49}$ erg (Campana et al. 2006). If such a burst was associated with SN 2010ay, its peak emission may have been a factor of four below the BAT sensitivity limit, although its total isotropic energy emission is an order of magnitude larger than our IPN limit for SN 2010ay. Finally, the event whose host galaxy and SN properties seem most similar to SN 2010ay, GRB 100316D/SN 2010bh, had $E_{\gamma,\mathrm{iso}} \geqslant (5.9 \pm 0.5) \times 10^{49}$ erg (Starling et al. 2011)—a full order of magnitude above our IPN limit.

Another possibility is that prompt emission associated with SN 2010ay may have been too soft to be detected by the BAT or IPN. For example, the spectrum of XRF 060218 rose to a peak at 0.3–10 keV at ~ 985 s after triggering and then softened significantly thereafter. Even though the total emission of this burst is well above our IPN limit, it may have escaped detection if it was similarly soft.

6. SUB-SOLAR HOST ENVIRONMENT METALLICITY

We estimate the oxygen abundance of the host environment of SN 2010ay from the strong nebular emission line fluxes measured from our Gemini spectrum (Table 3). At the distance

of the host galaxy, the 1″ Gemini slit width corresponds to a physical size of 1.3 kpc. The properties we infer for the explosion site of SN 2010ay represent a luminosity-weighted average over this radius.

We employ several different oxygen abundance diagnostics in order to determine the metallicity of the host galaxy from its optical spectrum (e.g., Modjaz et al. 2011). From the O3N2 diagnostic of Pettini & Pagel (2004, PP04), we derive a metallicity of log(O/H) = 8.19, or $Z \sim 0.3 Z_\odot$, adopting the solar metallicity log(O/H)$_\odot$ + 12 = 8.69 from Asplund et al. (2005). Using the N2 diagnostic of PP04, we find log(O/H) + 12 = 8.26. Using the abundance diagnostic, $R_{23} = \log([\mathrm{O\,II}]\,\lambda 3727 + [\mathrm{O\,III}]\,\lambda\lambda 4959, 5007)/\mathrm{H}\beta$, we find log(O/H) + 12$_{Z94}$ = 8.49 (Zaritsky et al. 1994) and log(O/H) + 12$_{KD02}$ = 8.50 (Kewley & Dopita 2002). However, these R_{23}-based estimates are more sensitive to flux calibration and reddening correction. Moreover, there is a well-known bi-valued relationship between R_{23} and oxygen abundance. The value $R_{23} = 0.873 \pm 0.006$ measured at the explosion site places it near the turnover point, but we assume that it lies on the upper branch based on its [N II]/[O II] ratio, following Kewley & Ellison (2008). The metallicity values we derive using the PP04 and KD02 diagnostics are approximately equivalent given the offset that exists between these two diagnostics (Kewley & Ellison 2008). These measurements are similar to the values reported by Modjaz et al. (2010) (log(O/H)+12 [PP04, KD02] = [8.2, 8.4]) for the SN 2010ay host galaxy. The statistical errors in our strong-line metallicity estimates are small (<0.01 dex), as determined by propagating the errors in the line flux measurement through the abundance calculation. However, for example, the representative systematic error for the PP04 O3N2 abundance diagnostic is ~ 0.07 dex, as determined by Kewley & Ellison (2008) via comparison to other strong-line abundance indicators.

Fortunately, our detection of the weak [O III] $\lambda 4363$ auroral line (S/N ~ 6; Figure 3) allows us to derive an oxygen abundance via the "direct," T_e method. We employ a methodology similar to that used by, for example, Levesque et al. (2010a). We first derive the electron temperature ($T_e = (1.09 \pm 0.06) \times 10^4$ K) and density ($n_e = 80 \pm 20$ cm^{-3}) from the [O III] and [S II] line ratios using the `temden` task of the IRAF package `nebular` (Shaw & Dufour 1994), derive the O$^+$ temperature using the calibration of Garnett (1992), and finally estimate the O$^+$ and O^{++} abundances following Shi et al. (2006). The direct abundance, log(O/H) + 12 = 8.24 ± 0.08, is in good agreement with the PP04 O3N2 value. The stated uncertainty reflects the propagation of the uncertainties for the line flux measurements. Indeed, the offset between these two diagnostics should be very small at this metallicity (Kewley & Ellison 2008).

We estimate the star formation rate (SFR) of the host galaxy using the Hα relation of Kennicutt (1998). After correcting for host galaxy extinction, we measure the Hα luminosity from our Gemini spectrum (Table 3) and estimate SFR = 1.1 $M_\odot$ yr^{-1}.

6.1. Blue Compact Galaxy Host

We compare the host galaxy of SN 2010ay to the nearby galaxy population of the SDSS spectroscopic survey. The physical properties of the host galaxy, SDSS J123527.19+270402.7, are estimated in the MPA/JHU catalog.[24] The total (photometric) galaxy stellar mass (M_*) is given as $3.6^{+2.9}_{-1.3} \times 10^8\,M_\odot$,

----

[24] http://www.mpa-garching.mpg.de/SDSS (described in Kauffmann et al. 2003; Tremonti et al. 2004; Brinchmann et al. 2004; Salim et al. 2007, and updated for SDSS DR7).

the aperture-corrected SFR is $1.0^{+0.3}_{-0.2}$ $M_\odot$ yr^{-1}, and the nuclear (fiber) oxygen abundance (O/H$_o$) is log(O/H) + 12 = $8.58^{+0.02}_{-0.03}$ on the scale of Tremonti et al. (2004, T04). The specific star formation rate (SSFR) of the host galaxy is then $\approx 2.8^{+0.9}_{-0.4}$ Gyr^{-1}. For consistency, we consider these values of M_*, the oxygen abundance, and the SFR for the host galaxy of SN 2010ay when comparing to other galaxies in the MPA/JHU catalog.

The oxygen abundance and SFR of the host galaxy of SN 2010ay listed in the MPA/JHU catalog are consistent with the values we derive in this paper (see also Kelly & Kirshner 2011). The MPA/JHU catalog lists metallicities on the T04 scale. Using the Kewley & Ellison (2008) conversion to the PP04 scale, the T04 metallicity estimate corresponds to a metallicity of log(O/H) + 12 = 8.38, which is ∼0.2 dex higher than the one we measure (log(O/H) + 12 = 8.19). However, there is a large (∼0.2 dex) rms scatter between the PP04 O3N2 and T04 diagnostics at the regime of log(O/H)+12$_{PP04}$ ∼ 8.2 (Kewley & Ellison 2008). The SFR in the MPA/JHU catalog is also in good agreement with the value we estimate from the Hα luminosity. Although our estimate does not include an aperture correction, the size of the Gemini slit (1) should encompass most of the star formation in the galaxy (Petrosian $r = 1.''355$; Table 1).

The mass-to-light ratio of the host galaxy of SN 2010ay is low compared to typical star-forming galaxies. To compare the host galaxy to the general galaxy population, we select a subset of the MPA/JHU catalog by requiring that estimates of M_*, SFR, and O/H$_o$ be available, and we remove active galactic nuclei (AGNs) according to Kauffmann et al. (2003). We consider 167,837 starbursting galaxies following these constraints. The host galaxy ranks in the [4th, 38th, 11th] percentile in [M_*, SFR, O/H$_o$] among these galaxies. Among the selected galaxies with a stellar mass as low as the host galaxy,[25] the median and standard deviation of the B-band[26] absolute magnitude are -15.8 ± 1.3 mag. With $M_B = -18.35 \pm 0.05$ mag, the host of SN 2010ay is more luminous than other galaxies with a similar mass at the 2σ level. The discrepancy is due to the blue color of the SN 2010ay host galaxy, which indicates a stellar population that is very young and therefore has a low stellar-mass-to-light ratio. Among the 1184 galaxies in the MPA/JHU catalog that meet the constraints above and have a color similar to the host of SN 2010ay ($0.47 < u-r < 0.67$, from SDSS fiber magnitudes), the host galaxy has typical properties, with [M_*, SFR, O/H$_o$] in the [46th, 49th, 54th] percentile.

Based on these properties, we classify the host galaxy of SN 2010ay as a luminous blue compact galaxy (BCG). BCGs span a large range in luminosity ($-21 < M_B < -12$, where luminous BCGs have $M_B < -17$) but are distinguished by their blue colors ($B - V < 0.45$), high SFR ($1 < $ SFR < 20 $M_\odot$ yr^{-1}), and low metallicity ($Z_\odot/50 < Z < Z_\odot/2$; Kunth & Östlin 2000; Kong & Cheng 2002). The host galaxy of SN 2010ay has a luminosity ($M_B = -18.35 \pm 0.05$), color ($B - V = 0.11 \pm 0.07$), SFR ($1.0^{+0.3}_{-0.2}$ $M_\odot$ yr^{-1}), and metallicity ($Z \sim 0.3$ $Z_\odot$) consistent with all these ranges.[27]

---

[25] This subset is selected such that the host galaxy of SN 2010ay has the median mass: $1.39 < M_* < 5.62 \times 10^8$ $M_\odot$, $N_{sim} = 6,978$.
[26] We obtain B-band magnitudes by converting the k-corrected gri magnitudes given in the MPA/JHU catalog to BVR magnitudes using the transformation of Blanton & Roweis (2007).
[27] We note that a large fraction of luminous BCGs show evidence for disturbed morphologies or interaction with close companions (Garland et al. 2004; López-Sánchez et al. 2006), but we do not see evidence for a companion at the depth of SDSS images of the host galaxy of SN 2010ay.
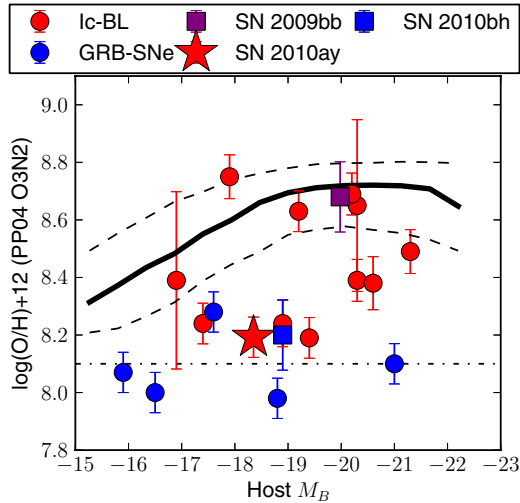
6.2. Comparison to SN Ic-BL and GRB–SN Host Galaxies

Our measurement of the metallicity from the Gemini spectrum indicates that the explosion site of SN 2010ay is ∼0.5(0.2) dex lower in metallicity than the median SNe Ic (Ic-BL) in the sample of Modjaz et al. (2011). In that sample, the median PP04 O3N2 metallicity measured at the explosion site of SNe Ic is log(O/H) + 12 ≈ 8.7 and for Ic-BL is ≈8.4 dex, for 12 and 13 objects, respectively. If instead the KD02 metallicity is used, the median of the sample is ≈8.9 dex for SNe Ic (13 objects) and ≈8.7 dex for Ic-BL (15 objects), so the abundance of the SN 2010ay host galaxy is similarly low compared to the median.

The metallicity of the environment of SN 2010ay is more similar to previously studied nearby GRB–SN progenitors. A metallicity identical to our measurement was measured at the explosion site of SN 2010bh (Levesque et al. 2011): log(O/H) + 12 = 8.2. In the survey of Levesque et al. (2010a), and adding the measurement for SN 2010bh, the GRB–SN host galaxies have an average and standard deviation PP04 O3N2 metallicity of log(O/H) + 12 = 8.1 ± 0.1 on the PP04 scale, which is consistent with the SN 2010ay environment. Among the 17 LGRB host galaxies surveyed in Savaglio et al. (2009), the average metallicity is somewhat lower, $1/6$ $Z_\odot$ or log(O/H) + 12 ∼ 7.9, but these are at an average redshift of $z \sim 0.5$ that is much higher than SN 2010ay.

This evidence suggests that the host galaxy of SN 2010ay has chemical properties more consistent with LGRBs/GRB–SNe than SNe Ic-BL without associated GRBs; however, selection effects may mitigate this discrepancy. SNe found in targeted surveys of luminous galaxies have host galaxy properties biased toward higher metallicities, due to the luminosity–metallicity ($L-Z$) relation (Tremonti et al. 2004). LGRBs are found in an untargeted manner through their gamma-ray emission and therefore are not biased by this relation.

SN 2010ay joins a growing list of SNe Ic-BL that have been discovered in low-metallicity host galaxies. Given the systematic uncertainty in strong-line oxygen abundance diagnostics (∼0.07 dex), we will consider host galaxies with metallicity log(O/H)$_{PP04}$ + 12 < 8.3 ($Z \lesssim 0.4$ $Z_\odot$) to be in the low-metallicity regime of SN 2010ay. Among the 15 SNe Ic-BL (9 discovered by untargeted searches) in the surveys of Modjaz et al. (2008) and Modjaz et al. (2011), 4 were found in low-metallicity environments: SN [2007eb, 2007qw, 2005kr, 2006nx] at log(O/H)$_{PP04}$ + 12 = [8.26, 8.19, 8.24, 8.24]. All of these SNe were discovered by untargeted searches. Young et al. (2010) measure the metallicity of the host galaxy of the broad-lined Ic SN 2007bg to be log(O/H)$_{PP04}$ + 12 = 8.18, although this SN has light curve and spectral properties that distinguish it from normal SNe Ic-BL (Section 3.3). Furthermore, Arcavi et al. (2010) find that SNe Ic-BL are more common in dwarf ($M_r \geqslant -18$) host galaxies, which the authors attribute to a preference for lower metallicities.

The star formation properties of the host galaxy of SN 2010ay also resemble the host galaxies of LGRBs. If we consider those galaxies in the MPA/JHU catalog with masses similar to the host galaxy of SN 2010ay (as defined above), then the median SFR and O/H$_o$ of these galaxies is 0.13 $M_\odot$ yr^{-1} and log(O/H$_o$)+12 = 8.36, respectively. The host galaxy of SN 2010ay is in the [96th, 77th] percentile for [SFR, O/H$_o$] among these galaxies. This indicates that, while the host galaxy of SN 2010ay falls within 1σ of the mass–metallicity ($M-Z$) relation for star-forming galaxies, its SFR is extreme for its mass.

Figure 9. Plot of host galaxy metallicity vs. absolute B magnitude for SNe Ic-BL (red) and engine-driven explosions (blue). The $L - Z$ relation of nearby star-forming galaxies is plotted as a solid line, with the 15th and 85th percentile boundaries of the galaxy distribution (dashed lines). Here, we have transformed the k-corrected gri magnitudes from the MPA/JHU catalog to B band (Blanton & Roweis 2007) and converted the T04 metallicity values to the PP04 scale (Kewley & Ellison 2008), for the purpose of comparing it to metallicity measurements for SN host galaxies in the literature. The dot-dashed horizontal line is the divider between GRB–SNe and SNe Ic-BL host environments suggested by Modjaz et al. (2008). The host galaxy properties of GRB/SNe other than 2010ay are from the following references: Starling et al. 2011; Cano et al. 2011a (2010bh), Modjaz et al. 2011 (Ic-BL), Levesque et al. 2010d (2009bb), and Levesque et al. 2010a (other GRB–SNe). Error bars illustrate measurement uncertainty, when published, plus a 0.07 dex systematic uncertainty.

(A color version of this figure is available in the online journal.)

The 39 LGRB host galaxies in the survey of Savaglio et al. (2009) are similarly low in mass and have high SFRs, with an average stellar mass of $M_* \sim 10^9 \, M_\odot$ and SSFR $\sim 3.5 \, \mathrm{Gyr}^{-1}$.

The host galaxy of SN 2010ay falls below the $L - Z$ relation for nearby star-forming galaxies, as illustrated by Figure 9. We have transformed the k-corrected gri magnitudes from the MPA/JHU catalog to B band (Blanton & Roweis 2007). At the luminosity of the host galaxy of SN 2010ay, the median metallicity and standard deviation of the SDSS galaxies on the T04 scale are $\log(\mathrm{O/H}) + 12 = 8.93 \pm 0.17$; the host galaxy of SN 2010ay falls in the 3rd percentile. In other words, the host galaxy of SN 2010ay is a 2σ outlier from the $L - Z$ relation. Similarly, Levesque et al. (2010a) and Han et al. (2010) suggest that the host galaxies of LGRBs fall below the $L - Z$ relation as defined by normal star-forming galaxies, BCGs, and the host galaxies of SNe Ic.

Mannucci et al. (2011) have explained the offset of LGRB host galaxies from the $M - Z$ relation as a preference for LGRBs to occur in host galaxies with high SFR, as characterized by the fundamental metallicity relation (FMR) of Mannucci et al. (2010; see also Lara-López et al. 2010). Using the extended FMR for low-mass galaxies from Mannucci et al. (2011), the host galaxy of SN 2010ay should have a metallicity of $\log(\mathrm{O/H}) + 12 = 8.20$ given its stellar mass and SFR. The FMR is calibrated to the Nagao et al. (2006) metallicity scale, which is similar to that of PP04 at this metallicity. Given the intrinsic scatter in the extended FMR on the order of ~ 0.05 dex, this value is consistent with the PP04 value we measure from our Gemini spectrum: $\log(\mathrm{O/H}) + 12 = 8.19$. Kocevski & West (2011) similarly explain the offset of LGRB host galaxies from the $M - Z$ relation as an SFR effect but suggest that the long

GRB host galaxies have even higher SFR than would be implied by the FMR.

SN 2010ay is an example of an SN Ic-BL where the host galaxy is consistent with the $M - Z$ relation for star-forming galaxies but deviates from the $L - Z$ relation due to its low stellar-mass-to-light ratio (Section 6.1). Its 2σ discrepancy from the $L - Z$ relation would be hard to explain as an SFR rate effect alone because among galaxies in the MPA/JHU catalog without AGNs (as defined above) and with M_B within 0.1 mag of the host galaxy of SN 2010ay, the host galaxy has an SFR in the 26th percentile ($<1\sigma$ discrepancy).

7. DISCUSSION

SN 2010ay has all the hallmark features associated with GRB–SNe, and yet we find no evidence of a relativistic explosion to sensitive limits. We are able to place constraints on the energy, density, velocity, progenitor mass-loss rate, and gamma-ray flux of any GRB that may have been associated with it. In particular, we may rule out the association of a GRB that looks similar to any spectroscopically confirmed GRB–SN to date, except for XRF 060218.

The low metallicity of the host environment of SN 2010ay may be suitable for GRB jet formation in the "collapsar" model, but our observations strongly constrain any relativistic outflow (Sections 4 and 5). In MacFadyen & Woosley (1999), a high rate of rotation in the core of the progenitor is required to power a relativistic jet. A low metallicity is prescribed to suppress the line-driven winds that would deprive the core of angular momentum. Apparently supporting this model, Stanek et al. (2006) found that the isotropic prompt energy release of the GRB–SNe decreases steeply with metallicity, and other surveys have found observational evidence for the preferential occurrence of GRB–SNe in low-metallicity host galaxies (Fynbo et al. 2003; Prochaska et al. 2004; Sollerman et al. 2005; Modjaz et al. 2006; Wiersema et al. 2007; Christensen et al. 2008; Modjaz et al. 2008; Levesque et al. 2010a; Chornock et al. 2010; Starling et al. 2011). Challenging this view is the recent discovery of SN 2009bb, a broad-lined, engine-driven SN Ic found in a high-metallicity host environment (Soderberg et al. 2010; Levesque et al. 2010d; Pignata et al. 2011). In SN 2010ay, we have found the opposite case—a broad-lined SN Ic found in a low-metallicity host environment, but without any indication (via either radio or gamma-ray emission) of a central engine. The existence of SNe 2009bb and 2010ay emphasizes that progenitor metallicity is not the key factor that distinguishes GRB–SNe from broad-lined SNe Ic without associated relativistic ejecta.

We compare the absorption velocity of SNe Ic-BL and engine-driven SNe (GRB–SNe and SN 2009bb) to the metallicity of their host environments in Figure 10. This comparison emphasizes the diversity of explosion and host galaxy properties observed in both engine-driven SNe and SNe Ic-BL. The engine-driven SNe with the largest velocity gradients (2003dh, $\alpha = -0.9 \pm 0.1$; 2009bb, $\alpha = -0.86 \pm 0.08$) occur at metallicities different by a factor of five (2003dh, $\log(\mathrm{O/H}) + 12 = 8.0$; 2009bb, $\log(\mathrm{O/H}) + 12 = 8.7$ on the PP04 scale). Furthermore, the velocity gradient of engine-driven SNe seems to be uncorrelated with the velocity at late times; 2010bh ($\alpha = -0.22 \pm 0.07$) and 2006aj ($\alpha = -0.3 \pm 0.2$) have similar velocity gradients, but 2010bh had velocities $\sim 10,000 \, \mathrm{km \, s}^{-1}$ larger at 30 days after explosion. Among SNe Ic-BL from low-metallicity environments ($\log(\mathrm{O/H}) + 12 < 8.5$), there is a large range in both the characteristic velocity and velocity gradient ($v_{\mathrm{Si}}^{30} = [10 \pm 1, 9 \pm 2, 21 \pm 2]$ and $\alpha = [-0.5 \pm 0.2, -0.3 \pm 0.2,$
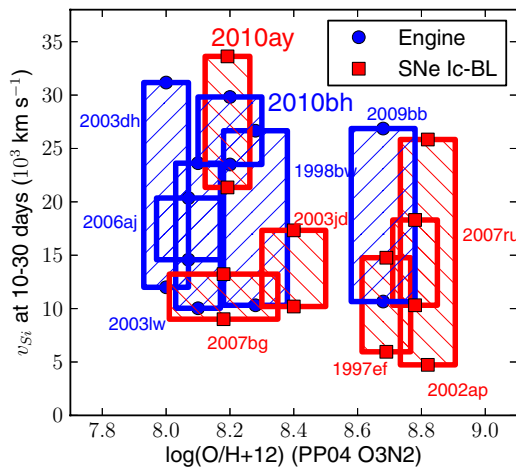
Figure 10. SN absorption velocity, as traced by the Si II λ6355 feature, vs. host galaxy oxygen abundance for SN 2010ay and other Ic-BL (red) and engine-driven explosions (blue) from the literature (as in Figure 5). The range of velocities hatched for each object comes from the velocity at 10 days and at 30 days after explosion, according to the power-law fits presented in Figure 5. The oxygen abundance measurements using the PP04 O3N2 diagnostic are from Levesque et al. (2010a; GRB–SNe), Sahu et al. (2009; SN2007ru), Young et al. (2010; SN 2007bg), and Modjaz et al. (2011; other SNe Ic-BL). The range of oxygen abundance hatched reflects the error bars quoted in the literature (when stated) plus the ∼0.07 dex systematic error of the PP04 O3N2 diagnostic (Kewley & Ellison 2008).

(A color version of this figure is available in the online journal.)

Table 5
Comparison between SN 2010ay and GRB 100316D/SN 2010bh

Property	SN 2010bh	SN 2010ay
Host galaxy properties		
$\log(O/H)+12^a$	8.2	8.19
Redshift (z)	0.059	0.06717
M_R	−18.5	−18.94
Explosion properties		
SN type	Ic-BL	Ic-BL
v_{Si}^{30} (10^3 km s^{-1})^b	24 ± 3	21 ± 2
M_R	-18.60 ± 0.08	-20.2 ± 0.2
M_{Ni} ($M_\odot$)	0.10 ± 0.01	$0.9^{+0.1}_{-0.1}$
M_{ej} ($M_\odot$)	1.93–2.24	$\gtrsim 4.7$
$E_{K,51}$	12.0–13.9	$\gtrsim 10.8$
GRB energy (E_{iso}, erg)	$\gtrsim 5.9 \times 10^{49c}$	$\lesssim 6 \times 10^{48}$

Notes. The observed properties of SN 2010bh and its host galaxy are given by Chornock et al. (2010), and light-curve modeling was performed by Cano et al. (2011a). The properties of SN 2010ay are derived in this paper.
^{a} The oxygen abundance derived from the PP04 O3N2 metallicity diagnostic, as discussed in Section 6.
^{b} The absorption velocity at 30 days after explosion, as measured from the Si II λ6355 feature in Section 3.
^{c} The lower limit of the total isotropic energy release estimated by Starling et al. (2011).

−0.4 ± 0.3] for SNe [2003jd, 2007bg, 2010ay]). For the three SNe Ic-BL at higher metallicities, the characteristic velocities tend to be lower and the velocity gradients tend to be stronger ($v_{Si}^{30} = [6 \pm 2, 5 \pm 2, 10.3 \pm 0.7]$ and $\alpha = [-0.8 \pm 0.4, -1.5 \pm 0.7, -0.5 \pm 0.1]$ for SNe [1997ef, 2002ap, 2007ru]). However, a larger sample is needed to exclude the possibility of SNe Ic-BL from super-solar metallicity environments that have high characteristic velocities or shallow velocity gradients.

The fact that a GRB was not detected in association with SN 2010ay, despite its similarities to the GRB–SNe, could indicate that the relativistic jet produced by this explosion was "suffocated" before it emerged from the progenitor star (MacFadyen et al. 2001). In this scenario, the duration of the accretion event onto the newly formed central engine is short-lived and the jet post-breakout outflow is not ultrarelativistic. In the process of being suffocated, the jet transfers momentum to the ejecta such that the spectrum is broad lined and the ejecta velocity is very high, even at late times, as we observe (Section 3). However, the low host environment metallicity we measure for SN 2010ay, which is similar to GRB–SNe, does not suggest high angular momentum loss that would help to weaken the jet. Another alternative is that binary interaction plays a key role in the commonality of relativistic outflows among SNe Ic-BL.

Looking forward, additional SNe Ic-BL in sub-solar metallicity host environments will be found through current and future generations of untargeted transient searches. Untargeted searches are required to find SNe from low-metallicity host environments, because targeted searches only probe the highest metallicity galaxies due to the luminosity–metallicity relationship (Modjaz et al. 2011; Leloudas et al. 2011).

8. CONCLUSIONS

The optical photometric and spectroscopic, radio, and gamma-ray observations of SN 2010ay presented here pro-

vide an example of a Type Ic-BL SN with explosion and host properties similar to the known GRB–SN 2010bh. This object demonstrates that SNe in low-metallicity environments with high-velocity ejecta are not necessarily accompanied by the traditional signature of radio emission associated with long-lived relativistic jets. The existence of SN 2010ay and SN 2009bb (a central-engine-driven event from a high-metallicity host environment) indicates that progenitor metallicity may not be the key factor that distinguishes GRB–SNe from normal broad-lined SNe Ic.

We conclude the following:

1. Pre-discovery imaging of the SN 2010ay from the Pan-STARRS1 3π survey allows us to tightly constrain the early-time light curve of SN 2010ay (see Figure 2) and explosion date (2010 February 21.3 ± 1.3), allowing us to search for gamma-ray emission that may have been associated with the explosion. By fitting the template SN Ib/c light curve of Drout et al. (2011), we derive an R-band peak absolute magnitude of −20.2 ± 0.2 mag—making SN 2010ay among the most luminous SNe Ib/c ever observed. This peak magnitude suggests that a large mass of nickel, $M_{Ni} \sim 0.9^{+0.1}_{-0.1} M_\odot$, has been synthesized. We estimate a ratio of M_{Ni} to M_{ej} that is ∼2 times larger than in known GRB–SNe.

2. Spectroscopy (see Figure 3) at the explosion site in the host galaxy of SN 2010ay indicates that the host environment of the progenitor star had a significantly sub-solar metallicity ($Z \sim 0.3 Z_\odot$), similar to the host environments of known GRB–SN progenitors.

3. The Type Ic-BL SN 2010ay strongly resembles the GRB–SN 2010bh, particularly in light of its unusually high absorption velocities at late times ($v_{Si} \approx 19.2 \times 10^3$ km s^{-1} at 14 days after peak) and low-metallicity host environment. The comparison between these two SNe is summarized in Table 5.

14

4. Non-detections in late-time EVLA radio observations of the SN rule out the association of a GRB of the nature of the spectroscopically confirmed GRB–SNe, except for the radio afterglow associated with XRF 060218. Our radio observations imply limits on the velocity, energy, and density of any associated relativistic jet and the mass-loss rate of the progenitor (see Figures 4, 6–8). Additionally, no coincident gamma-ray emission was detected by satellites: the non-detection by the IPN indicates $E_\gamma \lesssim 6 \times 10^{48}$ erg, while the non-detection by the *Swift*-BAT indicates that the peak energy of the burst was $\lesssim 1 \times 10^{47}$ erg s^{-1} if the burst occurred during the $\sim 20\%$ of the explosion window when it was in the field of view of the instrument. This rules out associated prompt emission similar to that of GRBs 031203, 030329, or 100316D, but not GRBs 980425 or 060218.

The pre-discovery imaging of SN 2010ay demonstrates the capability of the untargeted PS1 survey for identifying and monitoring exotic transients, not only in its high-cadence medium-deep fields but also in the all-sky 3π survey. Additional detections and multi-wavelength follow-up observations of SNe Ic-BL will help to illuminate the role that ejecta velocity and progenitor metallicity play in the GRB–SN connection.

REFERENCES

Abazajian, K. N., Adelman-McCarthy, J. K., Ageros, M. A., et al. 2009, ApJS, 182, 543
Aihara, H., Allende Prieto, C., An, D., et al. 2011, ApJS, 193, 29
Alard, C. 2000, A&AS, 144, 363
Arcavi, I., Gal-Yam, A., Kasliwal, M. M., et al. 2010, ApJ, 721, 777
Arnett, W. D. 1982, ApJ, 253, 785
Asplund, M., Grevesse, N., & Sauval, A. J. 2005, in ASP Conf. Ser. 336, Cosmic Abundances as Records of Stellar Evolution and Nucleosynthesis, ed. T. G. Barnes, III & F. N. Bash (San Francisco, CA: ASP), 25
Barthelmy, S. D., Barbier, L. M., Cummings, J. R., et al. 2005, Space Sci. Rev., 120, 143
Berger, E., Kulkarni, S. R., Frail, D. A., & Soderberg, A. M. 2003a, ApJ, 599, 408
Berger, E., Kulkarni, S. R., Pooley, G., et al. 2003b, Nature, 426, 154
Blanton, M. R., & Roweis, S. 2007, AJ, 133, 734
Blondin, S., Dessart, L., Leibundgut, B., et al. 2006, AJ, 131, 1648
Brinchmann, J., Charlot, S., White, S. D. M., et al. 2004, MNRAS, 351, 1151
Campana, S., Mangano, V., Blustin, A. J., et al. 2006, Nature, 442, 1008
Cano, Z., Bersier, D., Guidorzi, C., et al. 2011a, ApJ, 740, 41
Cano, Z., Bersier, D., Guidorzi, C., et al. 2011b, MNRAS, 413, 669
Cardelli, J. A., Clayton, G. C., & Mathis, J. S. 1989, ApJ, 345, 245
Chatzopoulos, E., Wheeler, J. C., & Vinko, J. 2009, ApJ, 704, 1251
Chevalier, R. A. 1982, ApJ, 258, 790
Chevalier, R. A. 1998, ApJ, 499, 810
Chevalier, R. A., & Fransson, C. 2006, ApJ, 651, 381
Chevalier, R. A., & Irwin, C. M. 2011, ApJ, 729, L6
Chomiuk, L., Chornock, R., Soderberg, A. M., et al. 2011, ApJ, 743, 114
Chornock, R., et al. 2010, arXiv:1004.2262
Christensen, L., Vreeswijk, P. M., Sollerman, J., et al. 2008, A&A, 490, 45
Conley, A., Howell, D. A., Howes, A., et al. 2006, AJ, 132, 1707
Drake, A. J., Djorgovski, S. G., Mahabal, A., et al. 2009, ApJ, 696, 870
Drake, A. J., Djorgovski, S. G., Mahabal, A., et al. 2010, CBET, 2224, 1
Drout, M. R., Soderberg, A. M., Gal-Yam, A., et al. 2011, ApJ, 741, 97
Filippenko, A. V., Silverman, J. M., Kleiser, I. K. W., & Morton, A. J. L. 2010, CBET, 2224, 3
Frail, D. A., Soderberg, A. M., Kulkarni, S. R., et al. 2005, ApJ, 619, 994
Frail, D. A., Waxman, E., & Kulkarni, S. R. 2000, ApJ, 537, 191
Fruchter, A. S., Levan, A. J., Strolger, L., et al. 2006, Nature, 441, 463
Fryer, C. L., & Heger, A. 2005, ApJ, 623, 302
Fukugita, M., Ichikawa, T., Gunn, J. E., et al. 1996, AJ, 111, 1748
Fynbo, J. P. U., Jakobsson, P., Möller, P., et al. 2003, A&A, 406, L63
Gal-Yam, A., Mazzali, P., Ofek, E. O., et al. 2009, Nature, 462, 624
Gal-Yam, A., Ofek, E. O., & Shemmer, O. 2002, MNRAS, 332, L73
Galama, T. J., Vreeswijk, P. M., van Paradijs, J., et al. 1998, Nature, 395, 670
Garland, C. A., Pisano, D. J., Williams, J. P., Guzmán, R., & Castander, F. J. 2004, ApJ, 615, 689
Garnett, D. R. 1992, AJ, 103, 1330
Gehrels, N., Chincarini, G., Giommi, P., et al. 2004, ApJ, 611, 1005
Graham, J. F., Fruchter, A. S., Kewley, L. J., et al. 2009, in AIP Conf. Proc. 1133, Gamma-ray Burst: Sixth Huntsville Symposium, ed. C. Meegan, C. Kouveliotou, & N. Gehrels (Melville, NY: AIP), 269
Han, X. H., Hammer, F., Liang, Y. C., et al. 2010, A&A, 514, A24
Hjorth, J., Sollerman, J., Möller, P., et al. 2003, Nature, 423, 847
Hodapp, K. W., Siegmund, W. A., Kaiser, N., et al. 2004, Proc. SPIE, 5489, 667
Hu, J. Y., Qiu, Y. L., Qiao, Q. Y., et al. 1997, IAU Circ., 6783, 1
Hurley, K., Golenetskii, S., Aptekar, R., et al. 2010, in AIP Conf. Proc. 1279, Deciphering the Ancient Universe with Gamma-ray Bursts, ed. N. Kawai & S. Nagataki (Melville, NY: AIP), 330
Izzard, R. G., Ramirez-Ruiz, E., & Tout, C. A. 2004, MNRAS, 348, 1215

Kaiser, N., Aussel, H., Burke, B. E., et al. 2002, Proc. SPIE, 4836, 154
Kauffmann, G., Heckman, T. M., Tremonti, C., et al. 2003, MNRAS, 346, 1055
Kelly, P. L., & Kirshner, R. P. 2011, arXiv:1110.1377
Kennicutt, R. C., Jr. 1998, ARA&A, 36, 189
Kewley, L. J., & Dopita, M. A. 2002, ApJS, 142, 35
Kewley, L. J., & Ellison, S. L. 2008, ApJ, 681, 1183
Kinugasa, K., Kawakita, H., Ayani, K., et al. 2002, ApJ, 577, L97
Kocevski, D., & West, A. A. 2011, ApJ, 735, L8
Kocevski, D., West, A. A., & Modjaz, M. 2009, ApJ, 702, 377
Kong, X., & Cheng, F. Z. 2002, A&A, 389, 845
Kulkarni, S. R., Frail, D. A., Wieringa, M. H., et al. 1998, Nature, 395, 663
Kunth, D., & Östlin, G. 2000, A&AR, 10, 1
Lara-López, M. A., Cepa, J., Bongiovanni, A., et al. 2010, A&A, 521, L53
Law, N. M., Kulkarni, S. R., Dekany, R. G., et al. 2009, PASP, 121, 1395
Leloudas, G., Gallazzi, A., Sollerman, J., et al. 2011, A&A, 530, A95
Levesque, E. M., Berger, E., Kewley, L. J., & Bagley, M. M. 2010a, AJ, 139, 694
Levesque, E. M., Berger, E., Soderberg, A. M., & Chornock, R. 2010b, ApJ, 709, L26
Levesque, E. M., Berger, E., Soderberg, A. M., & Chornock, R. 2011, ApJ, 739, 23
Levesque, E. M., Kewley, L. J., Graham, J. F., & Fruchter, A. S. 2010c, ApJ, 712, L26
Levesque, E. M., Soderberg, A. M., Foley, R. J., et al. 2010d, ApJ, 709, L26
Li, Z.-Y., & Chevalier, R. A. 1999, ApJ, 526, 716
López-Sánchez, Á. R., Esteban, C., & García-Rojas, J. 2006, A&A, 449, 997
MacFadyen, A. I., & Woosley, S. E. 1999, ApJ, 524, 262
MacFadyen, A. I., Woosley, S. E., & Heger, A. 2001, ApJ, 550, 410
Mannucci, F., Cresci, G., Maiolino, R., Marconi, A., & Gnerucci, A. 2010, MNRAS, 408, 2115
Mannucci, F., Salvaterra, R., & Campisi, M. A. 2011, MNRAS, 414, 1263
Mazzali, P. A., Deng, J., Pian, E., et al. 2006, ApJ, 645, 1323
Mazzali, P. A., Iwamoto, K., & Nomoto, K. 2000, ApJ, 545, 407
Modjaz, M., Filippenko, A. V., Silverman, J. M., Kleiser, I. K. W., & Morton, A. J. L. 2010, ATel, 2503, 1
Modjaz, M., Kewley, L., Bloom, J. S., et al. 2011, ApJ, 731, L4
Modjaz, M., Kewley, L., Kirshner, R. P., et al. 2008, AJ, 135, 1136
Modjaz, M., Stanek, K. Z., Garnavich, P. M., et al. 2006, ApJ, 645, L21
Nagao, T., Maiolino, R., & Marconi, A. 2006, A&A, 459, 85
Osterbrock, D. E., & Ferland, G. J. (ed.) 2006, Astrophysics of Gaseous Nebulae and Active Galactic Nuclei (2nd ed.; Sausalito, CA: University Science Books)
Pastorello, A., Smartt, S. J., Botticella, M. T., et al. 2010, ApJ, 724, L16
Patat, F., Cappellaro, E., Danziger, J., et al. 2001, ApJ, 555, 900
Perley, R., Napier, P., Jackson, J., et al. 2009, Proc. IEEE, 97, 1448
Pettini, M., & Pagel, B. E. J. 2004, MNRAS, 348, L59
Pian, E., Antonelli, L. A., Butler, R. C., et al. 2000, ApJ, 536, 778
Pignata, G., Stritzinger, M., Soderberg, A., et al. 2011, ApJ, 728, 14
Podsiadlowski, P., Mazzali, P. A., Nomoto, K., Lazzati, D., & Cappellaro, E. 2004, ApJ, 607, L17
Prieto, J. 2010, CBET, 2224, 3
Prieto, J. L., Stanek, K. Z., & Beacom, J. F. 2008, ApJ, 673, 999
Prochaska, J. X., Bloom, J. S., Chen, H.-W., et al. 2004, ApJ, 611, 200
Quimby, R. M., Kulkarni, S. R., Kasliwal, M. M., et al. 2011, Nature, 474, 487
Sahu, D. K., Tanaka, M., Anupama, G. C., Gurugubelli, U. K., & Nomoto, K. 2009, ApJ, 697, 676
Salim, S., Rich, R. M., Charlot, S., et al. 2007, ApJS, 173, 267
Sanders, N. E., et al. 2012, arXiv:1206.2643
Sari, R., Piran, T., & Narayan, R. 1998, ApJ, 497, L17
Savaglio, S., Glazebrook, K., & Le Borgne, D. 2009, ApJ, 691, 182
Sazonov, S. Y., Lutovinov, A. A., & Sunyaev, R. A. 2004, Nature, 430, 646
Schlegel, D. J., Finkbeiner, D. P., & Davis, M. 1998, ApJ, 500, 525
Shaw, R. A., & Dufour, R. J. 1994, in ASP Conf. Ser. 61, Astronomical Data Analysis Software and Systems III, ed. D. R. Crabtree, R. J. Hanisch, & J. Barnes (San Francisco, CA: ASP), 327
Shi, F., Kong, X., & Cheng, F. Z. 2006, A&A, 453, 487
Smartt, S. J. 2009, ARA&A, 47, 63
Soderberg, A. M. 2007, PhD thesis, Caltech
Soderberg, A. M., Chakraborti, S., Pignata, G., et al. 2010, Nature, 463, 513
Soderberg, A. M., Kulkarni, S. R., Berger, E., et al. 2004a, ApJ, 606, 994
Soderberg, A. M., Kulkarni, S. R., Berger, E., et al. 2004b, Nature, 430, 648
Soderberg, A. M., Kulkarni, S. R., Berger, E., et al. 2005, ApJ, 621, 908
Soderberg, A. M., Kulkarni, S. R., Nakar, E., et al. 2006a, Nature, 442, 1014
Soderberg, A. M., Kulkarni, S. R., Price, P. A., et al. 2006b, ApJ, 636, 391
Soderberg, A. M., Nakar, E., Berger, E., & Kulkarni, S. R. 2006c, ApJ, 638, 930
Sollerman, J., Östlin, G., Fynbo, J. P. U., et al. 2005, New Astron., 11, 103
Stanek, K. Z., Gnedin, O. Y., Beacom, J. F., et al. 2006, Acta Astron., 56, 333
Starling, R. L. C., Wiersema, K., Levan, A. J., et al. 2011, MNRAS, 411, 2792
Stoll, R., Prieto, J. L., Stanek, K. Z., & Pogge, R. W. 2012, arXiv:1205.2338
Stubbs, C. W., Doherty, P., Cramer, C., et al. 2010, ApJS, 191, 376
Tonry, J., & Onaka, P. 2009, Proceedings of the Advanced Maui Optical and Space Surveillance Technologies Conference, ed. S. Ryan (Maui: Maui Economic Development Board), E40
Tremonti, C. A., Heckman, T. M., Kauffmann, G., et al. 2004, ApJ, 613, 898
Valenti, S., Benetti, S., Cappellaro, E., et al. 2008, MNRAS, 383, 1485
Valenti, S., Taubenberger, S., Pastorello, A., et al. 2012, ApJ, 749, L28
van Eerten, H., Zhang, W., & MacFadyen, A. 2010, ApJ, 722, 235
van Eerten, H. J., & MacFadyen, A. I. 2011, ApJ, 733, L37
Waxman, E. 2004, ApJ, 602, 886
Wiersema, K., Savaglio, S., Vreeswijk, P. M., et al. 2007, A&A, 464, 529
Woosley, S. E., & Bloom, J. S. 2006, ARA&A, 44, 507
Woosley, S. E., & Heger, A. 2006, ApJ, 637, 914
Woosley, S. E., Langer, N., & Weaver, T. A. 1995, ApJ, 448, 315
Yoon, S.-C., Woosley, S. E., & Langer, N. 2010, ApJ, 725, 940
Young, D. R., Smartt, S. J., Mattila, S., et al. 2008, A&A, 489, 359
Young, D. R., Smartt, S. J., Valenti, S., et al. 2010, A&A, 512, A70
Zaritsky, D., Kennicutt, R. C., Jr., & Huchra, J. P. 1994, ApJ, 420, 87